

1-1-2012

Effects of plasma membrane cholesterol content on ultrasound and microbubble mediated sonoporation

Tetyana Yatsenko
Ryerson University

Follow this and additional works at: <http://digitalcommons.ryerson.ca/dissertations>

 Part of the [Biomedical Engineering and Bioengineering Commons](#), and the [Medical Biophysics Commons](#)

Recommended Citation

Yatsenko, Tetyana, "Effects of plasma membrane cholesterol content on ultrasound and microbubble mediated sonoporation" (2012). *Theses and dissertations*. Paper 707.

Effects of plasma membrane cholesterol content
on ultrasound and microbubble mediated
sonoporation

by

Tetyana Yatsenko

B.Sc. Medical Physics, Ryerson University, 2009

A thesis

presented to Ryerson University

in partial fulfillment of the

requirements for the degree of

Master of Science

in the Program of

Biomedical Physics

Toronto, Ontario, Canada, 2012

© Tetyana Yatsenko 2012

I hereby declare that I am the sole author of this thesis. This is a true copy of the thesis, including any required final revisions, as accepted by my examiners.

I authorize Ryerson University to lend this thesis to other institutions or individuals for the purpose of scholarly research.

I further authorize Ryerson University to reproduce this thesis by photocopying or by other means, in total or in part, at the request of other institutions or individuals for the purpose of scholarly research.

I understand that my thesis may be made electronically available to the public.

Effects of plasma membrane cholesterol content on ultrasound and microbubble mediated sonoporation

Master of Science 2012

Tetyana Yatsenko

Biomedical Physics

Ryerson University

Ultrasonically-stimulated microbubbles can increase cell membrane permeability and allow otherwise impermeable molecules to enter the intracellular space of cells; a phenomenon known as *sonoporation*. In this thesis, the effect of plasma membrane cholesterol content on modulating ultrasound-microbubble induced cell permeabilization and viability was investigated in an *in vitro* cell suspension model. Breast cancer cells (MDA-MB-231) with modified cholesterol content were exposed to ultrasound and microbubbles at varying acoustic pressures. The effect on cells was assessed through uptake of FITC-dextran (70kDa) and cell viability (propidium iodide marker) using flow cytometry. Ultrasound and microbubble induced permeabilization of cells depended on cholesterol content of the plasma membrane. The highest permeability of ~30% was achieved in unmodified cells compared to ~15% for cholesterol depleted cells at 1.5 MPa peak negative pressure. This study indicated that both addition and removal of cholesterol from cell plasma membrane results in decrease of ultrasound and microbubble induced permeabilization.

Acknowledgements

I would like to express my greatest gratitude to my supervisors Dr Raffi Karshafian and Dr Carl Kumaradas for guiding me through this project for the past two years. I want to thank Dr Kumaradas for granting me the position of the summer research assistant during the summer of 2006. That experience was extremely valuable to me; it showed me how much work it is required to do a research, it introduced me to amazing people from Prince Margaret Hospital, and finally, it helped me to understand what I want to do in my future. In addition, the opportunity to attend the CAP 2006 conference in Niagara Falls was very important to me and I appreciate it a lot. I would like to say special thanks to Dr Karshafian for his patience and tons of help with ultrasound settings, microbubble preparation, and flow cytometry analysis. Thank you, Dr Karshafian, for being at Ryerson on Saturdays and helping me to fix unexpected problems during the experiments. Moreover, I really appreciate your calm response to the yeast contamination issue. I am grateful to Dr Karshafian and Dr Kumaradas for providing constructive and critical responses to my work. It happened very often during those two years that I have certain thoughts on something but can't formulate them clearly; luckily for me both of my supervisors have this powerful ability to organize things in logical manner, which helped me to visualize the details as a part of a whole picture. It was a great pleasure to work with them. I learned not only about science, but also about the benefits of sharing your findings with others, about team work, and about how planning and setting short and long-term goals can bring the goal closer.

I would like to thank Dr Kolios for sharing his positive spirit and being in the committee. I would also like to thank Dr Botelho for being in the committee and for his useful comments on flow cytometry data analysis.

Special thanks goes to the Department of Physics at Ryerson University. Thanks to Arthur Worthington for his technical support, especially for his help with transducer calibration. I am very grateful to Dr Tavakkoli for allowing me to use his hydrophone. I very appreciate Dr Min Rui's help with cell related issues.

Thanks to all students from Dr Karshafian's lab for sharing the equipment peacefully and for supporting each other through our University experience. Special thanks to my family, especially my daughter Bianca and my husband Bogdan who survived all this years of me being a full-time student and provided their supports.

Dedication

Dedicated to my family

Contents

LIST OF FIGURES	IX
INTRODUCTION.....	1
1.1 PROBLEMS WITH ANTICANCER THERAPEUTIC AGENTS	1
1.2 INTRACELLULAR DELIVERY STRATEGIES FOR THERAPEUTIC AGENTS	2
1.3 ULTRASOUND AND MICROBUBBLES IN IMAGING AND THERAPY	4
1.3.1 <i>Physics of ultrasound</i>	5
1.3.2 <i>Diagnostic and therapeutic applications of ultrasound</i>	5
1.3.3 <i>Ultrasound microbubble contrast agents</i>	6
1.4 SONOPORATION	11
1.4.1 <i>Mechanism of sonoporation</i>	11
1.4.2 <i>Parameters affecting cell permeability and cell viability</i>	13
1.4.3 <i>Biological effects of ultrasound and microbubbles</i>	16
1.4.4 <i>Sonoporation applications</i>	18
1.5 BIOMECHANICAL PROPERTIES OF CELLS	19
1.6 CELL PLASMA MEMBRANE	19
1.6.1 <i>Composition and function of cell plasma membrane</i>	20
1.6.2 <i>Permeability and natural uptake of molecules by cells</i>	22
1.7 HYPOTHESIS AND OBJECTIVES.....	24
MATERIALS AND METHODS	25
2.1 <i>IN VITRO</i> CELL MODEL	25
2.2 DEPLETION AND LOADING OF PLASMA MEMBRANE CHOLESTEROL.....	26
2.3 ULTRASOUND AND MICROBUBBLES.....	27
2.3.1 <i>Ultrasound exposure system</i>	27
2.3.2 <i>Transducer characterization</i>	28
2.3.3 <i>Micobubble agent</i>	29
2.4 CELL PERMEABILITY AND CELL VIABILITY	30
2.5 THERAPEUTIC RATIO.....	35
2.6 RELATIVE PERMEABILITY AND RELATIVE VIABILITY	35
RESULTS: SONOPORATION OF MDA-MB-231 CELLS	36
3.1 CELL PERMEABILITY AND CELL VIABILITY	37
3.2 THERAPEUTIC RATIO.....	39
3.3 RELATIVE PERMEABILITY	40
3.4 RELATIVE VIABILITY	42
DISCUSSION	44
4.1 SONOPORATION AND PLASMA MEMBRANE	45
4.2 LIMITATIONS OF THIS STUDY.....	50
CONCLUSIONS AND FUTURE WORK.....	52
5.1 CONCLUSIONS.....	52
5.2 FUTURE WORK.....	52
5.2.1 <i>Sonoporation of PC3 cells</i>	53
5.2.2 <i>Measuring cholesterol content of cell plasma membrane</i>	59
APPENDIX A.....	60
A.1 <i>Cell permeability and cell viability of MDA-MB-231 cells</i>	60
A.2 <i>Therapeutic Ratio of MDA-MB-231 cells</i>	65

<i>A.3 Relative Permeability of MDA-MB-231 cells.....</i>	<i>69</i>
<i>A.4 Relative Viability of MDA-MB-231 cells.....</i>	<i>72</i>
REFERENCES	75

List of Figures

Figure 1.1: Stable (a) and transient (inertial) (b) cavitation of microbubbles in ultrasound field as a function of time.	9
Figure 1.2: Fluid mosaic model for membrane structure	21
Figure 1.3: Cholesterol intercalates between fatty acid chains of phospholipids	22
Figure 2.1: Ultrasound exposure apparatus	27
Figure 2.2: (a) Micropositioning system , (b) Side view of exposure chamber with acoustically transparent window.....	28
Figure 2.3: 1MHz transducer calibration curve.	29
Figure 2.4: Fluorescent spectra of FITC-dextran and PI	32
Figure 2.5: a. Flow cytometry data analysis for control (0MPa) and b. for ultrasound treated (1.5 MPa) MDA-MB-231 cells.	33
Figure 3.1: The effect of plasma membrane modification with cholesterol loading and depletion on cell permeability of MDA-MB-231 cells from experiments repeated four times.	37
Figure 3.2: The effect of plasma membrane modification with cholesterol loading and depletion on cell viability of MDA-MB-231 cells from experiments repeated four times.....	38
Figure 3.3: The effect of plasma membrane modification with cholesterol loading and depletion on therapeutic ratio of MDA-MB-231 cells from experiments repeated four times.	39
Figure 3.4: The effect of the plasma membrane modification with cholesterol loading and depletion on relative permeability of MDA-MB-231 cells at 0.5 and 1.5 MPa.	41
Figure 3.5: The effect of the plasma membrane modification with cholesterol loading and depletion on relative viability of MDA-MB-231 cells at 0.5 and 1.5 MPa. Each bar represents mean relative viability for a given plasma membrane condition (unmodified, cholesterol loaded and cholesterol depleted) and pressure (0.5 and 1.5 MPa).	43
Figure 5.1: The effect of the plasma membrane modification with cholesterol loading and depletion and peak negative pressure on cell permeability of PC3 in experiment 5 (n=6).	54
Figure 5.2: The effect of the plasma membrane modification with cholesterol loading and depletion and peak negative pressure on cell viability of PC3 in experiment 5 (n=6). T	55
Figure 5.3: The effect of the plasma membrane modification with cholesterol loading and depletion and peak negative pressure on the therapeutic ratio of PC3 in experiment 5 (n = 6).	56
Figure 5.4: The effect of the peak negative pressure and the plasma membrane modification with cholesterol loading and depletion on relative permeability of PC3 cells in Experiment #5.	57
Figure 5.5: The effect of the peak negative pressure and the plasma membrane modification with cholesterol loading and depletion on relative viability of PC3 cells in Experiment #5.....	58

Figure A.1: The effect of the plasma membrane modification with cholesterol depletion and peak negative pressure on cell permeability and cell viability of MDA-MB-231 in experiment 1 ($n=4$).	62
Figure A.2: The effect of the plasma membrane modification with cholesterol loading and peak negative pressure on cell permeability and cell viability of MDA-MB-231 in experiment 2 ($n=8$).	63
Figure A.3: The effect of the plasma membrane modification with cholesterol loading and depletion and peak negative pressure on cell permeability and cell viability of MDA-MB-231 in experiment 3 ($n=4$).	63
Figure A.4: The effect of the plasma membrane modification with cholesterol loading and depletion and peak negative pressure on cell permeability and cell viability of MDA-MB-231 in experiment 4 ($n=4$).	64
Figure A.5: The effect of the plasma membrane modification with cholesterol depletion and peak negative pressure on the therapeutic ratio of MDA-MB-231 in experiment 1 ($n=4$).	67
Figure A.6: The effect of the plasma membrane modification with cholesterol loading and peak negative pressure on the therapeutic ratio of MDA-MB-231 in experiment 2 ($n=8$).	67
Figure A.7: The effect of the plasma membrane modification with cholesterol loading and depletion and peak negative pressure on the therapeutic ratio of MDA-MB-231 in experiment 3 ($n=4$).	68
Figure A.8: The effect of the plasma membrane modification with cholesterol loading and depletion and peak negative pressure on the therapeutic ratio of MDA-MB-231 in experiment 4 ($n=4$).	68
Figure 3.9: The effect of the plasma membrane modification with cholesterol loading and depletion on relative permeability of MDA-MB-231 cells at 0.5 MPa for three independent experiments.	71
Figure 3.10: The effect of the plasma membrane modification with cholesterol loading and depletion on relative permeability of MDA cells at 1.5 MPa for four independent experiments.	71
Figure A.11: The effect of the plasma membrane modification with cholesterol loading and depletion on relative viability of MDA-MB-231 cells at 0.5 MPa for three independent experiments.	73
Figure 3.13: The effect of the plasma membrane modification with cholesterol loading and depletion on relative viability of MDA-MB-231 cells at 1.5 MPa for four independent experiments.	74

Chapter 1

Introduction

The efficiency of drug-based therapies, whose aim is to exhibit therapeutical effect on target cells, is limited by the inability of many pharmaceuticals to cross the plasma membrane (Larkin et al. 2008). Various biophysical and biochemical methods have been employed to overcome the plasma membrane barrier to deliver pharmaceuticals intracellularly (Gao X et al. 2007, Kim et al. 2008, Liu et al. 2003, Madeira et al. 2011). The focus of this thesis is on the intracellular delivery modality known as sonoporation, which employs ultrasound with microbubbles to create transient pores on the surface of the plasma membrane. This allows pharmacologically active, non-permeable molecules to cross the cell membrane. Sonoporation applications have been tested for thrombolysis (Meunier et al. 2007), cancer treatment (Nomikou and McHale, 2010), cardiovascular treatment (Miller et al. 2002), and treatments involving passage of pharmaceuticals across the blood-brain barrier (Mears and Alonso 2007, Mayer et al. 2008). However, the consistent and controllable delivery of pharmaceuticals remains a challenge due in part to the lack of knowledge about the mechanisms of sonoporation.

1.1 Problems with anticancer therapeutic agents

Cancer is the second major cause of death in the USA after cardiovascular diseases (Globcan 2008, IARC 2010). All affected cells should be killed to treat cancer successfully. Radiation combined with chemotherapy is a common approach to cancer

treatment. Furthermore, in certain cases solid tumors can also be removed surgically. Effectiveness of radiation therapy and chemotherapy is limited due to a lack of specificity, heterogeneous distribution of pharmaceutical within a tumor, and abnormal tumor vasculature (Rapoport et al. 2009, Wang Binghe et al. 2005, Ward et al. 1991).

Chemotherapy is a molecular-based therapy aimed at delivering pharmaceuticals at a precise site of action at a desired concentration (Wang et al. 2005). The site of action for the majority of existing drugs is inside the cell (Frenkel 2008). Therefore, efficiency of molecular-based therapies and chemotherapy in particular, depends on the ability to deliver therapeutic agents intracellularly.

For any method of administration, pharmaceutical encounter barriers on their way to the target. For example, high interstitial pressure and the presence of fibrillar collagen in the extracellular matrix of solid tumors are barriers that decrease drug delivery efficiency *in vivo* (Frenkel 2008). In addition, molecular based therapies are limited by the toxic side effects on healthy tissues. Furthermore, the cell's plasma membrane creates a physiological barrier, which prohibits complex pharmaceuticals, such as proteins, silencing RNAs, DNA, enzymes, and other therapeutic compounds, to enter inside the cell (Schlicher et al. 2006, Torchilin 2006). Therefore, various strategies are being investigated with the aim to increase the efficiency of intracellular delivery of therapeutically active molecules.

1.2 Intracellular delivery strategies for therapeutic agents

Intracellular delivery methods can be subdivided into viral and non-viral methods. Viral methods (Warrington Jr. and Herzog 2006) use vectors that are highly efficient. However, the low loading capacity of recombinant viruses and safety concerns with

potential to cause immunogenic and cytotoxic reactions limit their applications. Non-viral delivery methods employ various chemical and physical approaches to deliver pharmaceuticals into the cell. Chemical methods are based on cellular uptake of carriers via endocytosis, such as micelles, liposomes, and polymers, loaded with pharmaceuticals. Those methods aim to reduce undesired interactions of pharmaceuticals with normal tissues. Additionally, conjugation of targeting ligands on the surface of carriers improves delivery precision. The drawback of chemical methods is a lack of stability of loaded carriers (Liu et al. 2003) and toxicity (Gao X et al. 2007). The delivery precision can be significantly improved if chemical carriers can be activated precisely at the target. This can be achieved by the external application of ultrasound to the target area (Karshafian et al. 2009).

Physical approaches make use of mechanical devices, electrical and ultrasonic energy. Such methods use physical force to create transient defects on the cell plasma membrane, so that pharmaceuticals can enter the cell. One such example is the gene gun, a mechanical device that accelerates gold particles loaded with pharmaceuticals by pressurized gas (Yang et al. 1990). It efficiently delivers pharmaceuticals intracellularly within a confined area, but has a low penetration depth of only a few millimeters, limited loading capacity of gold particles, and difficulties with *in vivo* applications.

An electric field of short duration and high voltage facilitates the formation of reversible pores on the plasma membrane, a process called electroporation (Gehl 2003). The novel method of electroporation (Kim et al. 2008), which utilizes capillary and wire type electrodes, can create transient pores in up to 80% of the cells exposed to the electric field with cell viability up to 70-80%. On the other hand, *in vivo* applications of

electroporation are limited by restricted effective range (~ 1 cm) between the electrodes (Madeira et al. 2011). Those electrodes should be positioned deep inside the internal organs in order to treat those organs, which require surgery. In addition thermal heating can cause irreversible tissue damage (Gehl 2003).

The focus of this thesis is on intracellular delivery of impermeable molecules facilitated by ultrasound. The formation of reversible pores on the surface of the plasma membrane of target cells, induced by ultrasound exposure, is called sonoporation (Deng et al. 2004). Those transient pores on the surface of the plasma membrane, known as membrane permeabilization, allows pharmaceuticals, otherwise impermeable, to get inside the cell.

There are numerous advantages in using ultrasound for intracellular drug delivery. Firstly, it is non-invasive, and in *in vivo* applications ultrasound can be sharply focused deep within the body with millimeter precision to produce a localized effect (Chapelon et al. 2000). Secondly, it can be applied externally, endoscopically, or intravascularly. Finally, ultrasound, as an imaging modality, can be used to guide and monitor therapeutic applications in real time *in vivo*

1.3 Ultrasound and microbubbles in imaging and therapy

Ultrasound and microbubbles have been utilized for diagnostic and therapeutic applications in medicine and biology. Diagnostically, when microbubbles are used as an ultrasound contrast agents they enhance the detection of small vessels in both normal and malignant tissues and subsequently improve detection and assess treatment response

(Lindner 2004). In addition, application of ultrasound and microbubbles is being investigated for sonoporation (Karshafian et al. 2009).

1.3.1 Physics of ultrasound

Ultrasound is a mechanical pressure wave with frequencies above 20 kHz. Waves are defined as transverse or longitudinal based on the direction of particle displacement, with respect to the direction of propagation. In transverse waves, which are typical for solid materials, the oscillations of the particles are perpendicular to the direction of propagation. In longitudinal waves, which are typical for fluids and tissues, oscillation of the particles is parallel to the direction of propagation (Cobbold 2007).

The speed of ultrasound propagation is affected by mass, spacing, and attracting forces between the particles. The speed of ultrasound propagation depends on temperature, ultrasound frequency, tissue anisotropy and composition (Duck 1990). When ultrasound propagates through the tissue it loses energy through attenuation, resulting in the absorption and scattering of the wave. Ultrasound can penetrate deep inside the body (except lung and bone). This ultrasound property results in its use in a variety of fields, in medical imaging in particular, where the reflected ultrasound signal provides information about the tissue's structure (Kirk Shung 2006).

1.3.2 Diagnostic and therapeutic applications of ultrasound

Ultrasound imaging is non-invasive, safe, and a well-established technique, which allows for the determination of acoustic properties of soft tissue and blood flow in large vessels. Soft tissue acoustic properties, such as density and compressibility can be

obtained from A-mode, B-mode, M-mode, 3D, and 4D imaging (Szabo 2004). Doppler imaging has been used to determine movement of blood and to visualize it. In addition, therapeutic applications make use of low-intensity ultrasound for drug delivery (sonophoresis, sonoporation), sonothrombolysis, and gene therapy while high-intensity ultrasound is used for physiotherapy, lithotripsy, and histotripsy (Yu et al. 2004).

The extent of ultrasound induced bio-effects, either thermal or non-thermal, depends on ultrasound exposure parameters. Thermal bio-effects are attributed to the heating capacity of the ultrasound beam, which attenuates during propagation in tissue (Cobbold 2007). Part of ultrasound energy is absorbed by tissue, resulting in an increase of tissue temperature. Non-thermal effects include radiation pressure and acoustic cavitation and are not associated with heating. Radiation pressure is defined as a unidirectional force created in the direction of ultrasound propagation. Acoustic cavitation is the interaction of an acoustic wave with a gas filled microbubble (Brujan 2004). Microbubbles can be naturally present in the body in relatively large liquid compartments, such as the urinary and cardiovascular systems, or they can be created during ultrasound exposure, or introduced into the body artificially as contrast agents (Kimmel 2006).

1.3.3 Ultrasound microbubble contrast agents

Microbubble composition

Ultrasound contrast agents, or microbubbles, are gas-encapsulated bodies composed of a shell and a gas filled core with a diameter of 1-5 μ m (Qin et al. 2009). The shell of microbubbles are comprised of a thin 10-200 nm layer that acts as a barrier between the aqueous and gas phases, reducing surface tension and preventing gas

diffusion from the core. The shell can be composed of lipids, proteins or polymers. In a lipid shell the structure of the carbon side chain covalently attached to hydrophilic head group determine surface viscosity, gas permeation resistance, and buckling stability (Kim et al. 2008). The lipid shell structure is not uniform (Borden et al. 2005). The microbubble shell contains microdomains separated by defects or grain boundaries, which affects its mechanical properties and acoustic response. Protein-shell microbubbles were designed to carry targeting ligands and/or a genetic payload (Lindner 2004). The microbubbles core is composed of gases of higher molecular weight (denser) compared to air, such as octafluoropropane, perfluorocarbon or sulphur hexafluoride (Bull 2007).

Microbubbles in ultrasound fields

When microbubbles are placed in an ultrasound field with a pressure above a particular amplitude threshold, the microbubbles will either oscillate or be disrupted (Mayer et al. 2008). Microbubble behavior in ultrasound field depends on ultrasound exposure parameters (such as peak negative acoustic pressure, pulse centre frequency, pulse duration, pulse repetition frequency, and insonation time), physical properties of microbubbles, such as size and composition, and surrounding environment (Krasovitski and Kimmel 2007). When acoustic pressure is low, microbubbles experience stable cavitation and oscillate in a linear mode. Microbubbles emit an acoustic pressure wave, which characteristics depend on microbubble properties and ultrasound exposure parameters. Microbubbles undergo maximum oscillation at their resonance frequency, which depends on microbubble size and shell properties (Ferrara et al. 2007).

A microbubble in a fluid exposed to ultrasound can create two types of fluid flow: streaming and microstreaming (VanBavel 2007). Streaming is facilitated by radiation

force, which may cause microbubble translocation in various directions including away from ultrasound source (primary radiation force), toward each other (secondary radiation force or Bjerknes force), and toward the nodes and antinodes in a standing wave (Kimmel 2006). Microstreaming is the form of streaming that occurs around a microbubble with velocities and shear rates proportional to the amplitude of microbubble, oscillation.

Microbubbles can be disturbed by ultrasound through outward diffusion of the gas during the compression phase, diffusion of the gas through shell defects, or through an inertial cavitation mechanism (Ferrara et al. 2007). At higher pressures microbubbles that undergo expansion become unstable and collapse during the application of negative pressure phase (Figure 1.1). The collapsing microbubbles fragment into smaller bubbles. Smaller bubbles serve as cavitation nuclei, which also increase in size and eventually collapse again. Microbubbles in incompressible fluids collapse symmetrically. The pattern of microbubble collapse changes if it is placed in the vicinity of a rigid boundary. Based on numerical simulation (Brujan 2004), where it is assumed the liquid around the microbubble is inviscid, incompressible and irrotational, the position of the microbubble and the dynamic behavior of the jet around the bubble was found to be dependent on the distance between microbubble and the boundary as well as the amplitude of the pressure wave.

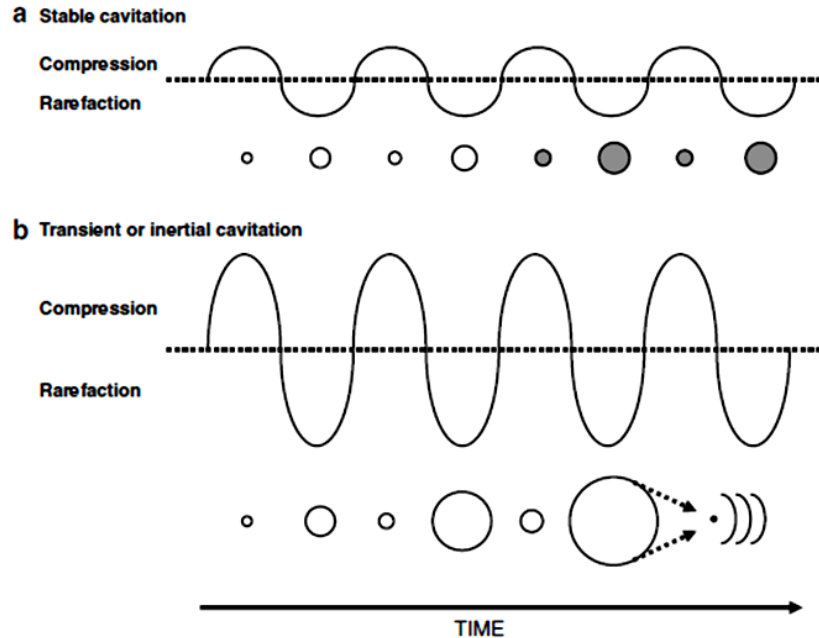


Figure 1.1: Stable (a) and transient (inertial) (b) cavitation of microbubbles in ultrasound field as a function of time.

Inertial cavitation mechanisms cause bubbles to disrupt after significant radial expansion. The process of microbubble collapse is accompanied by significant increase in local pressure (up to hundreds MPa) and temperature (up to thousands of Kelvin) (Liang et al. 2011). Collapsing microbubbles generates spherical shockwaves around themselves. The location of microbubble collapse in biological tissues has significant impact in terms of generated bio-effects. Microbubble cavitation in a semi-infinite space (like bladder and heart ventricles) has been studied extensively. For example, Krasovitski and Kimmel (2001) numerically modeled microbubbles in a thin semi-infinite liquid film between boundaries, such as cavities of the peritoneum. The most complicated case is when microbubbles are located near cells that are 2-3 times greater than microbubble diameter. In this case, collapse is asymmetrical and can result in the formation of liquid microjets (Sheguang Zhang et al. 1993).

Microbubbles as pharmaceutical carriers

Loading microbubbles with pharmaceutical agents results in enhanced delivery of those pharmaceuticals (Frenkel et al. 2002). Pharmaceuticals can be loaded either onto the microbubble shell surface, or into subsurface inner layer, or into the interior of microbubble (Mukherjee et al. 2000, Linder 2004). In addition to increased delivery efficiency, microbubble loading opens the opportunity to deliver nucleic acids and proteins, that otherwise will be destroyed in the blood stream.

Targeting of microbubbles

Microbubbles can be targeted to specific cells to improve the therapeutic effect of pharmaceuticals by ensuring high concentrations of the pharmaceutical at the target while reducing the pharmaceutical's toxicity to healthy tissues (Liang et al. 2010). The challenges associated with targeting include, but are not limited to the atypical vasculature of tumor. However, *in vitro* targeting was accomplished using the electrostatic interaction between a hepatocarcinoma-specific monoclonal antibody and liposome-based microbubbles (Bian et al. 2004). Finally, microbubbles, capable of targeting cancer cells in circulation were developed (Simberg and Mattrey 2009). The adhesion between target cells and the immune-microbubbles in un-fractionated whole blood was highly specific, which makes this method very promising for control of metastasis or treating certain conditions such as leukemia.

The combined application of ultrasound and microbubbles has a potential to facilitate intracellular delivery of pharmaceuticals by increasing the permeability of cell plasma membranes (Karshafian et al. 2009). This process is called sonoporation.

1.4 Sonoporation

Sonoporation is a phenomenon that describes the application of ultrasound with microbubbles to create transient pores on the surface of the plasma membrane. This allows pharmacologically active, non-permeable molecules to cross the cell membrane. The advantage of sonoporation aided drug delivery is that drugs can be released locally with a high level of precision. It is non-invasive, portable, and a relatively cheap technique that can be applied externally to the treated area (Szabo 2004). Sonoporation induced drug and gene therapy has been tested for cancer (Nomikou and McHale 2010), cardiovascular treatment (Miller et al. 2002), and treatments involving delivery of pharmaceuticals across the blood-brain barrier (Mears and Alonso 2007, Mayer et al. 2008). The outcome of sonoporation is usually described in terms of cell permeability (percentage of permeabilized cells that remain viable), cell viability, and therapeutic ratio (ratio of permeabilized to non-viable cells) (Karshafian et al. 2009). Currently sonoporation-mediated treatments are limited by low cell permeability. Ultimately the goal of sonoporation is to maximize percentage of permeabilized and viable cells while minimizing percentage of dead cells.

1.4.1 Mechanism of sonoporation

It is believed that the main biological mechanism underpinning sonoporation is formation of the transient pores on the surface of the plasma membrane. The sizes of the pores have been shown to vary from 2 nm up to hundreds of nanometers (Taniyama et al. 2002). Experimentally, it was found that the pore size distribution is likely to be heterogeneous with small pores more abundant than large ones (Mehier-Humbert et al.

2005). Pores remain open for a very short period of time, and particles, whose sizes are below the pore size, can enter the cell. The cell's plasma membrane reseals itself in a period ranging from tenths of seconds (Taniyama et al. 2002) to a few seconds (Zhao et al. 2008) following ultrasound exposure. The process of resealing requires Ca^{2+} to enter the cell through ultrasound-induced pores (Deng et al. 2004).

Acoustical mechanisms responsible for sonoporation are related to the effects associated with stable and transient (inertial) microbubble oscillations. Stable oscillations cause formation of microstreams and shock waves (Lentacker et al. 2009). Microstreams and shock waves induce strain on nearby cell membranes (Marmottant and Hilgenfeldt 2003). Microstreams and shock waves may also rupture pharmaceutical-loaded carriers, resulting in local release of pharmaceuticals. Transient microbubble oscillations is followed by violent collapse and accompanied by formation of microjets and shock waves. The latter may transiently permeabilize cell plasma membrane by piercing it (Ohl et al. 2006) and/or inflicting large mechanical stress on the cell. Transient permeabilization may result in the intracellular delivery of pharmaceutical.

Microbubbles loaded with pharmaceuticals have a potential to enhance intracellular delivery even more. When ultrasound is applied microbubbles fragment and its contents, drugs or/and genes are released locally. This prevents the spread of pharmaceutical from treated area, which is important when cytotoxicity of normal cells must be considered. Consequently, the concentration of released pharmaceutical is also higher next to permeabilized cells, which ensure that the maximum amount of pharmaceutical molecules pass through pores into the cells (Frenkel 2008).

The local delivery of pharmaceutical drug molecules using ultrasound and microbubbles can be achieved through different approaches. In the first approach therapeutic agents, loaded on microbubbles or co-administered with microbubbles, are injected into blood stream. The application of ultrasound can cause not only the permeabilization of endothelial cells, but also a release of the enclosed therapeutic agents in microvasculature, which lead to a local increase in pharmaceutical concentration and increased extravasation of pharmaceutical (Qin et al. 2009). Cells in the extravascular space can be targeted with ultrasound and microbubbles by locally injecting the pharmaceutical agent, as was demonstrated through intramuscular injection (Li et al. 2003). In a more novel approach, perfluorocarbon nanodroplets were administered intravenously and due to their small size of less than 500 nm they leaked passively out of the tumor vasculature into the extravascular space (Fan et al. 2006). In another study (Rapoport et al. 2009), nanodroplets were injected directly into the tumor. Nanodroplets in ultrasound field can be converted into microbubbles that subsequently facilitate tumor cell permeabilization and intracellular delivery of pharmaceutical drug molecules.

1.4.2 Parameters affecting cell permeability and cell viability

Sonoporation studies have been conducted under varying ultrasound delivery methods, conditions, and cell types (Deng et al. 2004, Karshafian et al. 2009, Mehier-Humbert et al. 2005, Pan et al. 2005). There has been a large variation in cell permeability between studies, which makes it difficult to compare results. However, the factors that affect cell permeability can be grouped into ultrasound exposure parameters,

microbubble properties, type of pharmaceutical to be introduced inside the cell, and most probably, cell plasma membrane mechanical properties.

Ultrasound exposure parameters

Cell permeability is affected by ultrasound exposure parameters including acoustic pressure, pulse centre frequency, pulse duration, pulse repetition frequency and insonation time. In general, cell permeability increases with acoustic pressure, reaches a maximum, following which permeability decreases (Karshafian et al. 2009, Liang et al. 2004). Higher ultrasound pressures cause more cell death (Deng et al. 2004). Exposure to lower frequencies results in higher percentage of permeabilized, as well as higher percentage of dead cells (Meijering et al. 2007). Cell permeability, as well as cell death, increases with pulse duration, pulse repetition frequency and insonation time. Karshafian et al. (2009) demonstrated that it is possible to optimize cell permeability *in vitro* and cell viability through adjustment of ultrasound exposure parameters.

Microbubble agent

Microbubble type (size, shell composition and core gas) and concentration play a role in sonoporation outcome (Blomley 2003, Wang et al. 2005, Karshafian et al. 2010, Li et al. 2003). *In vitro* experiments demonstrated that microbubble-to-cell ratio and microbubble-cell spacing influence cell permeability (Karshafian et al. 2009, Ward et al. 2000). Cells located closer to the microbubbles were more likely to die during ultrasound exposure.

Pharmaceutical properties

The size and type of pharmaceutical being delivered is important for cell permeability. Molecules with larger size (~ 470 kDa) were delivered intracellularly into rat mammary carcinoma cells (MAT B III) less efficiently than smaller molecules (77-164 kDa), which were probably related to the size of the pores on the plasma membrane (Mehier-Humbert et al. 2005). However, Karshafian et al. (2010) demonstrated that impermeable macromolecules, ranging in size from 10 kDa to 2 MDa were delivered to the intracellular space of KHT-C cells with similar efficiency. In another study, Liang et al. (2004) inferred linear relationship between plasmid concentration and nuclear DNA uptake in ultrasound mediated gene transfer in skeletal muscle cells.

Cell plasma membrane mechanical properties

Fahnestock et al. (1986) reported a differing response in insonation of two closely related murine C1300 neuroblastoma cell lines *in vitro*. The two cell lines differ mainly in their plasma membrane properties. Such results suggest that under the same ultrasound exposure conditions cells with different plasma membrane properties respond differently. Furthermore, Nozaki et al. (2003) tested the effect of membrane modification with lidocaine and temperature on ultrasound-mediated gene transfection. Lidocaine is a local anesthetic, which destabilizes plasma membranes by breaking the hydration shell and fluidizing lipid membranes and the temperature rise enhances membrane fluidity (Ueda et al. 1994). The results demonstrate that both the addition of lidocaine (1 mM) and the exposure to 42-44 °C temperature increase cell permeability following ultrasound and microbubble exposure by ~ 18-fold and 19 folds respectively.

1.4.3 Biological effects of ultrasound and microbubbles

Ultrasound and microbubble exposure can induce bioeffects on cells including cell lysis, cell membrane permeabilization, changes in cell size and passage of ions, endocytosis facilitation, and cytoskeleton reorganization. These effects may vary in cells with different composition of their plasma membranes.

Cell lysis and plasma membrane permeabilization

Plasma membrane wounding, which appeared after ultrasound and microbubble exposure, was studied on DU 145 prostate cancer cells and primary human astrocyte cells *in vitro* with electron and confocal microscopy, and flow cytometry (Schlicher et al. 2010). The outcome of wounding was either cell repair (transient permeabilization) or cell death due to the inability to reseal pores. At lower pressures poration of the plasma membrane in viable cells was observed (Taniyama et al. 2002). It has also been shown that, under certain exposure conditions, such as under higher peak negative acoustic pressure, ultrasound and microbubbles can cause cell death by cell lysis, which was demonstrated in cervical cancer cells (HeLa S3) *in vitro* (Ward et al. 1999).

Changes in cell size

In vitro experiments with Jurkat lymphocytes demonstrated that cell size was reduced after exposure to ultrasound and microbubbles, which could be explained by the leakage of cytosolic fluid through transient pores (Ross et al. 2002). Mehier-Humbert et al. (2005) observed through electron microscopy an ultrasonic “shaving” effect immediately after insonation: the cell surface become smother due to the removal of surface macromolecules such as glycoproteins from the cell membrane. Ultrasound

exposure of human lymphocytes *in vitro* resulted in the removal of CD-19 surface receptor from the surface of the plasma membrane. In both cases the cell size reduction was due to the removal of a thin superficial layer from the plasma membrane.

Change in ion passage

Hydrogen peroxide (H₂O₂, an oxidizing agent composed of oxygen-oxygen single bond), which can be produced during microbubble collapse in ultrasound field, plays a role in calcium permeability. Ultrasound and microbubble exposure induce an influx of calcium ions in bovine aortic endothelial cells (Meijering et al 2009), cardiomyoblast cells (Juffermans et al 2006), *Xenopus* oocytes (Pan et al 2005), and Chinese hamster ovary cells (Kumon et al 2007).

Endocytosis facilitation

The involvement of endocytosis in sonoporation was investigated by Meijering et al. (2009) on primary endothelial cells with dextran molecules ranging from 4.4 kDa to 500 kDa. They hypothesized that endocytosis, as well as pore formation is a key mechanism in ultrasound mediated targeted delivery. Moreover, the contribution of endocytosis depends on the molecular size of dextran; bigger molecules (155-500 kDa) are more likely to enter the cell via endocytosis, and smaller molecules (up to 70 kDa) by pore formation.

Cytoskeleton reorganization

F-actin stress fibers in human umbilical vein endothelial cells *in vitro* become rearranged and increased in number following ultrasound and microbubbles exposure (Juffermans et al. 2009). Those changes were significantly diminished after 30 to 60

minutes following ultrasound exposure, suggesting that cell viability was not affected through ultrasound exposure.

1.4.4 Sonoporation applications

The therapeutic applications of sonoporation have been tested for various treatments, such as thrombolysis (Meunier et al. 2007), cancer treatment (Nomikou and McHale, 2010), cardiovascular treatment (Miller et al. 2002), and treatments involved in delivery of pharmaceuticals across the blood-brain barrier (Mearis and Alonso 2007, Mayer et al. 2008). It was demonstrated that administration of thrombolytic agents in combination with ultrasound and microbubbles enhanced dissolution of blood clots, a process known as thrombolysis (Meunier et al. 2007). Combination of sonoporation with chemotherapeutics, such as bleomycin, permits access of the chemotherapeutics to the intracellular space and enhances cell death *in vivo* (Larkin et al. 2008). The blood-brain barrier is impermeable to majority of pharmaceuticals, which makes treatment of brain tumors such as gliomas complicated. Local sonoporation creates transient disruptions of the blood-brain barrier and ensures delivery of anticancer pharmaceuticals to the interstitial space in the brain (Mearis and Alonso 2007). In addition, ultrasound in combination with bradykinin (pharmaceutical, which causes blood vessels to dilate) increase permeabilization of the blood-brain barrier by opening tight junctions, as demonstrated by Zhang et al. (2009) on C6-glioma rat model.

For all of the above applications, intracellular drug delivery is facilitated through transient disruptions on the plasma membrane surface. The biomechanical properties of target cells may play role in the permeabilization of their plasma membranes.

1.5 Biomechanical properties of cells

Cells are complex, dynamic, and heterogeneous structures. Various experimental techniques have demonstrated that cells have both elastic and viscous properties. Their stiffness is similar to a gelatin gel, but under steady stress they continue to deform (Kasza et al. 2007). Visco-elastic properties of eukaryotic cells are important for many biophysical and physiological responses and are mainly determined by cytoskeletal organization and plasma membrane structure (Cai et al. 2010).

The cytoskeleton is an interlocking, three-dimensional biopolymer network of actin, microtubules, and intermediate filaments. Its main functions are to maintain organization of the cytoplasm, to mediate cell motility and shape adjustments during cell cycle, and to generate mechanical forces within the cell (Nelson and Cox 2008). Each cytoskeletal component is composed of simple protein subunits, joined non-covalently. Their structure is constantly changing: filaments disassemble into their protein subunits and reassemble into filaments again. Multiple cross linkage of filaments and the highly nonlinear dynamic structure of the cytoskeleton make its studies very complex.

1.6 Cell plasma membrane

Cell plasma membrane, along with cytoskeleton, determines visco-elastic properties of eukaryotic cells. The plasma membrane maintains ion and chemical gradients, controls material exchange between the cell and its environment, due to its selective permeability, senses and controls communication between the cells, and maintains cell shape (Nelson and Cox 2009).

1.6.1 Composition and function of cell plasma membrane

Cell plasma membrane is approximately 5 nm thick and is predominantly composed of proteins, lipids, and oligosaccharides. The fluid mosaic model of the plasma membrane (Singer and Nicolson 1972) considers the membrane as a two-dimensional liquid where lipids and proteins diffuse easily and form heterogeneous structure (Figure 1.2). The main membrane lipids are phospholipids (glycerophospholipids and sphingophospholipids) and cholesterol (Figure 1.3). Phospholipids are oriented in a bilayer in such a way that the hydrophobic non-polar tails are pointing towards each other, while the hydrophilic polar phosphate heads are pointing towards the internal cytosolic and external surfaces.

Cholesterol (Figure 1.3) is a steroid that is known to maintain membrane structure and regulate membrane fluidity (Dibya et al. 2010). Plasma membrane fluidity is a broad term that describes the motional freedom of lipid-soluble molecular probes (like 1,6-diphenyl-1,3,5-hexatriene (DPH) used for the measurement of fluidity in cell plasma membranes) within the lipid bilayer. Membranes with higher cholesterol content have lower plasma membrane fluidity and vice versa (Lars Bastiaanse et al. 1997). Cholesterol's chemical structure dictates its orientation within phospholipids; its polar hydroxyl group interacts with phospholipid head groups, while a hydrophobic steroid ring is oriented parallel to the hydrocarbon chains of the phospholipid bilayer (Singer and Nicolson 1972, Bastiaanse et al. 1996). Cholesterol molecules immobilize the first few hydrocarbon groups of the phospholipids making bilayer less deformable. In addition, cholesterol prevents crystallization of hydrocarbons in fatty acid chains because part of its steroid ring is closely attracted to the part of the fatty acid chain on the closest

phocpholipid. The above structure leads to slight immobilization of the outer surface of the membrane, which makes it less soluble to the small water-soluble molecules, and prevents membrane from being overly fluid.

The amount of cholesterol in cell plasma membrane is kept at a narrow range for a given cell line and is determined by cholesterol influx and efflux, esterification, deesterification, and synthesis (Brown and Goldstein 1986).

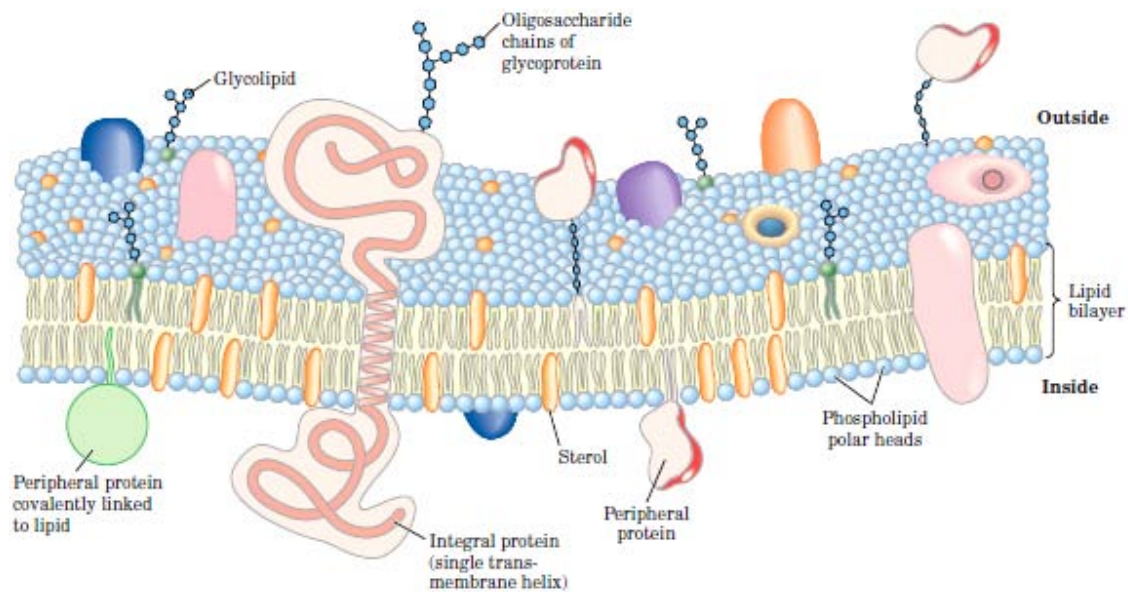


Figure 1.2: Fluid mosaic model for membrane structure (From Nelson David L., & Cox Michael M. (Eds.). (2008). From Principles of biochemistry (5th ed.), New York: W.H.Freeman and company.)

In previous studies (Needham et al. 1988, Kakorin et al. 2005) cholesterol was investigated as a chemical to induce a change in electrochemical membrane permeabilization: it reduced pore formation in small unilamellar bilayer vesicles placed in an electric field. Koronkiewicz & Kalinowski (2004) confirmed that cholesterol has a stabilizing effect on membrane bilayers: it increases the electric potential required for electroporation.

The cholesterol content of the plasma membrane, and therefore its fluidity can be modified. Previous studies (Goodwin et al. 2005, Lagerholm et al. 2005) demonstrated that it is possible to remove almost 50% of membrane cholesterol following by methyl β cyclodextrin (M β CD) treatment. In addition, treatment with cholesterol-loaded M β CD can triple initial membrane cholesterol concentration (Goodwin et al. 2005, Lagerholm et al. 2005). M β CD and cholesterol-loaded M β CD act from the surface of the plasma membrane without creating bonds or insertion into the plasma membrane (Klein et al. 1995).

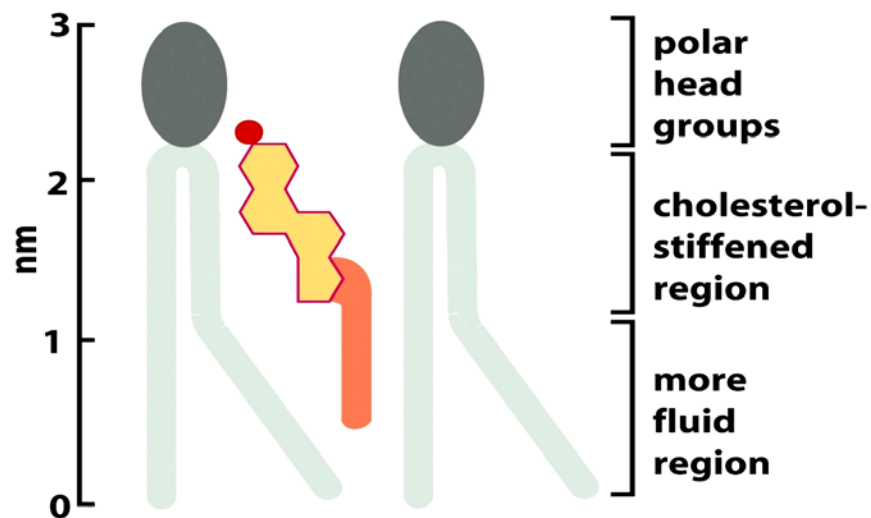


Figure 1.3: Cholesterol intercalates between fatty acid chains of phospholipids (Figure 10-5 Molecular Biology of the Cell (© Garland Science 2008))

1.6.2 Permeability and natural uptake of molecules by cells

The plasma membrane is selectively permeable. Some substances, such as certain gases (CO_2 , N_2 , O_2) and small uncharged polar molecules (water, urea, and ethanol) can diffuse through it. However, the transport of large polar molecules and ions across membranes can be subdivided into diffusion, passive transport, and active transport

(Nelson and Cox 2009). Some particles can enter the cell through endocytosis, a process of active consumption of particles by a cell. Complex multistage endocytic mechanisms are closely associated with lipid and protein composition of the plasma membrane (Doherty and McMahon 2009).

However, the above transport mechanisms cannot transport the majority of the currently available pharmaceuticals across the plasma membrane. Sonoporation, along with other intracellular delivery modalities, aimed to deliver impermeable pharmaceuticals across cell plasma membrane. Plasma membrane composition, its cholesterol content in particular, may be one of the factors influencing cell permeability.

1.7 Hypothesis and objectives

The hypothesis guiding this study was that the cholesterol content of the cell plasma membrane affects ultrasound-microbubble induced permeabilization. The hypothesis was tested using an *in vitro* cell suspension model and fluorescent markers with flow cytometry.

1.7.1 SPECIFIC OBJECTIVES:

- To measure the cell permeability and cell viability of *in vitro* cell suspensions of breast cancer (MDA-MB-231) cells with ultrasound and microbubbles and without ultrasound and microbubbles
- To determine the effect of the plasma membrane cholesterol on cell permeability and cell viability using those conditions described above.

Chapter 2

Materials and methods

Cells with modified cholesterol content of plasma membrane were exposed to ultrasound and microbubbles. The content of cell plasma membrane was modified by addition and removal of cholesterol from the plasma membrane. The effects of modification of plasma membrane cholesterol content on cell membrane permeability and viability after sonoporation were measured using fluorescent molecule diffusion and flow cytometry.

2.1 *In vitro* cell model

Cells in suspension were used as a biological model to investigate the effects of membrane modification on sonoporation. Breast cancer adenocarcinoma cells (MDA-MB-231) originated in the mammary gland were used.

Cells (MDA-MB-231) were grown in tissue culture flasks (660190 Greiner Bio-One, Germany) as a monolayer in RPMI growth media (31800 Gibco Invitrogen Inc, Canada) supplemented with 10% fetal bovine serum (12483 Gibco Invitrogen Inc, Canada,) at 37 °C, 5% CO₂, and 90% relative humidity prior to harvest during exponential growth by trypsinization. Prior to ultrasound treatment and membrane modification, cells were suspended in growth media at a concentration 0.6×10^6 cells/mL in a volume of 600 µL and kept at room temperature (~22 °C) during the experiment.

Cells were treated with cholesterol modifying agents in accordance with standard protocol (Goodwin et al. 2005, Lagerholm et al. 2005). Microbubbles and 70 kDa FITC-dextran (fluorescein isothiocyanatedextran, D-1822, Invitrogen Inc, Carlsbad, CA) were added to the cell suspension 60 seconds before ultrasound exposure. Cell membrane permeabilization was determined by the cellular uptake of 70kDa FITC-dextran, a cell impermeable fluorescent probe. A volume of 10 μ L of FITC-dextran at a concentration 7.7mg/mL was added to cell suspension to measure cell permeability (Karshafian et al 2010). Cell viability was determined with propidium iodine (PI) (P3566, Invitrogen Inc, Eugene, Oregon, USA). PI fluoresces only when bound to DNA, labeling non-viable cells. Following ultrasound treatment, cells were centrifuged and washed twice with FBS-free media. A volume of 5 μ L of PI at a concentration of 0.2 mg/mL was added to the cells and analyzed using flow cytometry.

2.2 Depletion and loading of plasma membrane cholesterol

Cholesterol was removed from cells using methyl- β -cyclodextrin (M β CD) based on a standard protocol (Goodwin et al. 2005, Lagerholm et al. 2005). Cells were washed with PBS, trypsinized, resuspended in serum-free growth media (RPMI 31800 Gibco Invitrogen Inc, Canada) and incubated for 40 min at 37 $^{\circ}$ C in the absence (control cells) or presence (treated cells) of 5mM M β CD (C4555-1G, Sigma, Germany). For cholesterol loading 5 mM of cholesterol, conjugated with M β CD (C4951, Sigma, Germany) was added to the cells resuspended in serum free growth media and incubated

for 40 min at 37 °C. Following cholesterol removal or loading, cells were exposed to ultrasound and microbubbles.

2.3 Ultrasound and microbubbles

2.3.1 Ultrasound exposure system

A schematic diagram of the ultrasound exposure apparatus is shown in Figure 2.1. The setup consisted of a 1 MHz centre frequency single element transducer (IL0108HP, Valpey Fisher Inc, Hopkinton, MA) mounted on micropositioning system (Figure 2.2 a), waveform generator (WW 5062, Tabor Electronics Ltd, Tel Hanan, Israel), power amplifier (240L, ENI Inc, Rochester, NY), oscilloscope (Tektronix Inc., Beaverton, OR, USA), and a cell exposure chamber (Figure 2.2 b) with acoustically transparent windows and a magnetic stirrer.

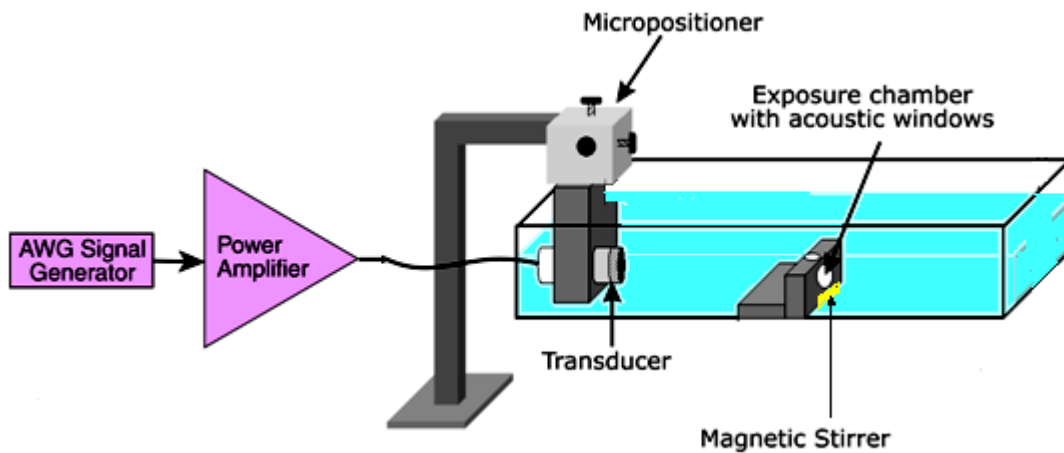
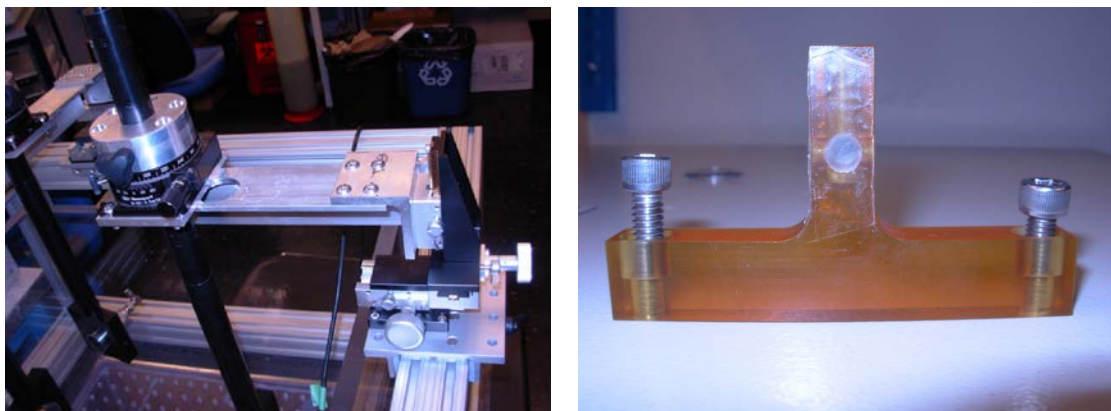


Figure 2.1: Ultrasound exposure apparatus: cells are placed into the exposure chamber with acoustically transparent window and mixed with magnetic stirrer during the treatment.



a.

b.

Figure 2.2: (a) Micropositioning system allows positioning of an ultrasound transducer (not pictured here) in 3 dimensions, (b) Side view of exposure chamber with acoustically transparent window.

The exposure apparatus tank was filled with degassed water. The cells in suspension were placed in the exposure chamber at the acoustic focus of the transducer and gently stirred with magnetic stirrer (Variomag) to ensure uniform ultrasound exposure of cell suspension. Cells were exposed to 1 MHz pulse center frequency, 16 cycles for 2 min insonation time, duty cycle of 1.6%, and peak negative acoustic pressures of 0.5 and 1.5 MPa.

2.3.2 Transducer characterization

A 1 MHz (IL0108HP, Valpey Fisher Inc, Hopkinton, MA) center frequency transducer with 25 mm element diameter focused at 70 mm was used in this study. The transducer was characterized using a calibrated needle hydrophone (Precision Acoustics Ltd., Dorchester, Dorset, UK). The pressure was measured at the focus of the transducer beam in the absence of the exposure chamber (Figure 2.3). The peak negative pressure was further used to characterize acoustic amplitude.

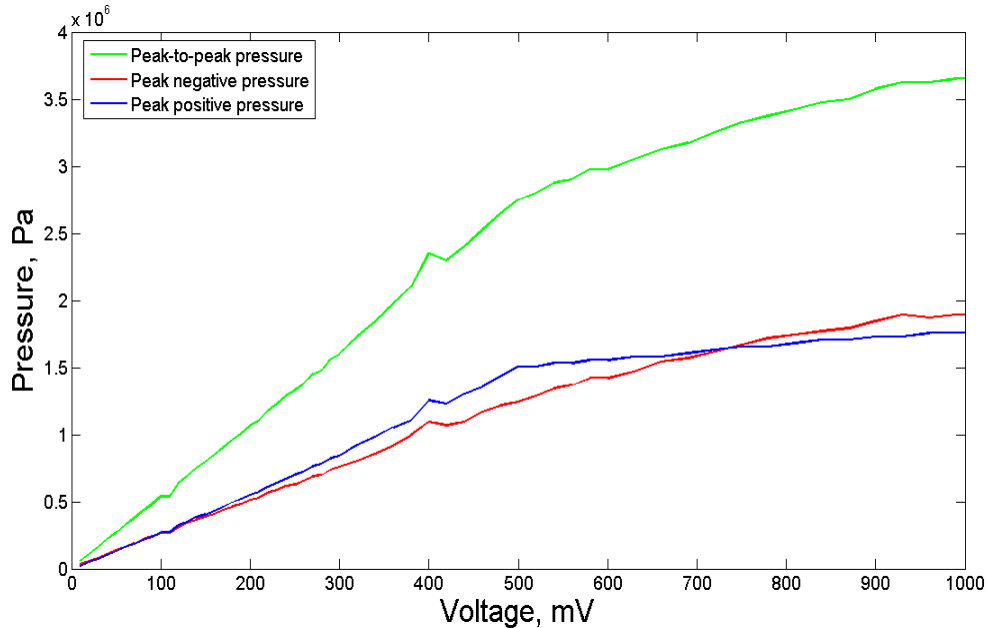


Figure 2.3: 1MHz transducer calibration curve. y-axis represent pressure in Pa, x-axis represents voltage in mV. Green curve is peak-to-peak pressure, red curve –absolute value of peak negative pressure, blue curve – peak positive pressure.

2.3.3 Micobubble agent

Definity, a clinically approved imaging contrast agent (Perflutren lipid microspheres, Lantheus Medical Imaging, Billerica, MA, USA), was used in this study. Definity microbubbles are composed of a phospholipid shell and octofluoropropane (C₃F₈) gas core. Definity has a concentration of 1.2x10¹⁰ bubbles/mL, a mean diameter of 1.1-3.3 μm with 98% less than 10 μm, and a maximum diameter of 20 μm according to the manufacturer (Lantheus Medical Imaging). Before activation, the Definity vial was kept at room temperature for 60 minutes to allow the vial temperature to equilibrate. The vial was activated by shaking using a Vial-Mix (Lantheus Medical Imaging, Billerica, MA, USA) for 45 seconds. The vial was kept at room temperature for 5 min after activation to equilibrate. The vial was rolled in between hands for 10 seconds, and then kept inverted for 30 seconds. Finally, it was vented with 18-gauge needle and

microbubbles were transferred to a syringe. Microbubbles were diluted with PBS in a ratio of 1:4.

2.4 Cell permeability and cell viability

Cell permeability and cell viability were determined after ultrasound exposure using fluorescent markers and flow cytometry (BD FACSCalibur, BD Biosciences International, San Jose, CA).

Flow cytometry is a cell counting technique based on the submersion of cells into a stream of fluid and analysis using electronic detection apparatus, which analyses fluctuations in brightness in scattered and fluorescent light. At the beginning light of a single wavelength is produced by a laser and hits the cell sample. One detector, which is aligned with the light beam (forward scatter), another detector, which is positioned perpendicularly to the light beam (side scatter), and four fluorescent detectors detect scattered and fluorescent light. Forward scatter is directly related to the cell volume, while side scatter reflects inner complexity of a cell such as membrane roughness and the amount of cytoplasmic granules. Certain proportion of the incident light is absorbed by the sample and some molecules from the sample fluoresce. Fluorescent detectors detect fluorescent light from those molecules and correlate the amount of fluorescence with the number of fluorescing cells.

The fluorescence spectrum of FITC-dextran and PI is shown in Figure 2.4. Flow cytometry was used to determine the viable cell permeability - number of cells stained with FITC-dextran but unstained with PI (upper left quadrant, UL), and cell viability. Cell viability was determined by subtracting non-viable cells, which are stained with PI

(sum of the count from upper right, UR and lower right, LR) from the total number of counted cells. Figure 2.5 demonstrated flow cytometry data from two MDA-MB-231 cell samples: an untreated sample (Figure 2.5 a.) and a sample treated with ultrasound and microbubbles at 1.5 MPa (Figure 2.5 b.) peak negative acoustic pressure.

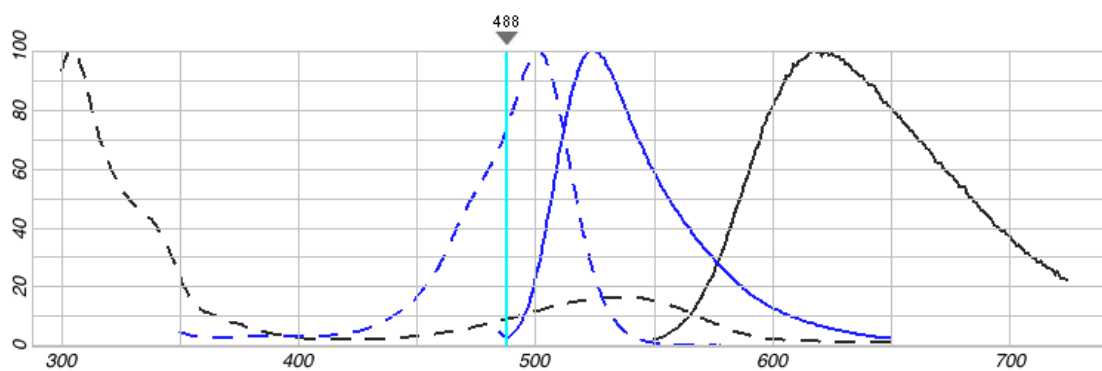


Figure 2.4: Fluorescent spectra of FITC-dextran (solid blue line is emission spectrum, dashed blue line is excitation spectrum) and PI (solid black line is emission spectrum, dashed black line is excitation spectrum). x-axis represents the wavelength (nm), y-axis represents a percentage of the maximum value for excitation and emission. The 488 nm laser created the excitation. Photomultipliers with with bandpass filters of 530 nm (for FITC-dextran) and 585 nm (for PI) were used to detect fluorescence. (From invitrogen.com)

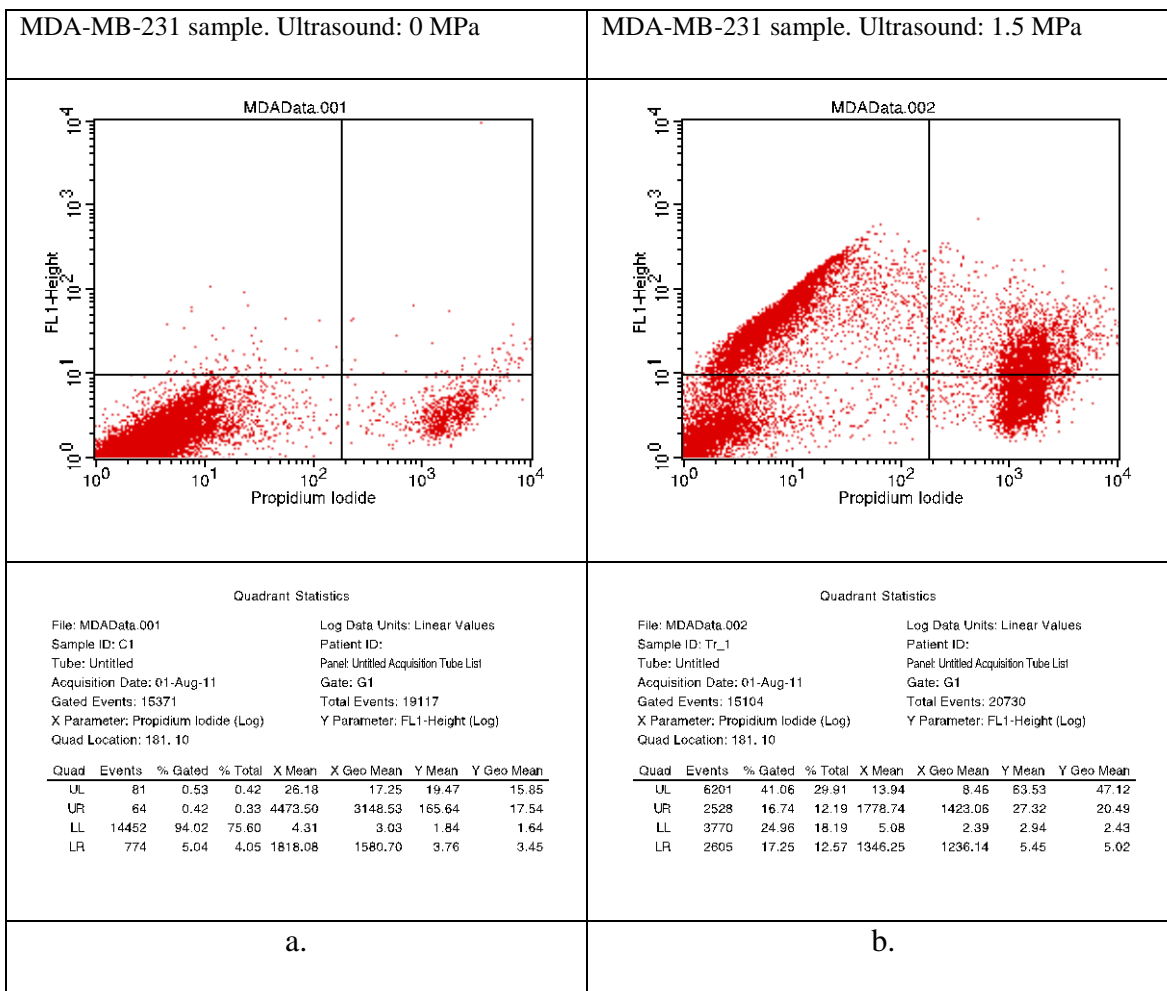


Figure 2.5: a. Flow cytometry data analysis for control (0MPa) and b. for ultrasound treated (1.5 MPa) MDA-MB-231 cells. Two-parameter histogram dot plot, displaying PI on the x-axis and FL1-FITC-dextran on the y-axis, is divided into four quadrants in accordance with the value of logarithmic x and y-axes. Cells are considered PI-negative if they appear in the range from 10^0 to 10^2 on the x-axis, cells that appear beyond 10^2 on the x-axis is PI-positive cells. FITC-positive cells will show on the y-axis starting from 10^1 , cells below this value are FITC-negative. Upper left quadrant contains cells, which are FITC-positive and PI-negative, lower left quadrant contains FITC-negative and PI-negative cells, upper right quadrant contains FITC-positive and PI-positive cells, while lower right quadrant contains FITC-negative and PI-positive cells. Tables in the second row represent statistical analysis for each sample. The entire cell population was gated based on the forward and side scatter diagram in order to eliminate count of the cellular debris and smaller particles. The percentage of gated events counted in the upper left (UL) quadrant was used to obtain the count of permeabilized and viable cells (sonoporation efficiency parameter). The percentage of dead cells was calculated by adding the percentage of FITC-Positive and PI-positive (UR) to FITC-negative and PI-positive (LR). Viability was found by subtracting percentage of dead cells from 100 %.

A count of 15000 cells was analyzed per sample. The data in terms of cell permeability and cell viability are presented individually from the following sonoporation experiments.

- Experiment 1: MDA-MB-231 unmodified and cholesterol depleted cells were exposed to 0, 0.5, 1.5 MPa peak negative acoustic pressure with the number of samples per condition, $n = 4$.
- Experiment 2: MDA-MB-231 unmodified and cholesterol loaded cells were exposed to 0, 0.5, 1.5 MPa peak negative acoustic pressure with $n = 8$.
- Experiment 3: MDA-MB-231 unmodified, cholesterol depleted, and cholesterol loaded cells were exposed to 0, 1.5 MPa peak negative acoustic pressure with $n = 4$.
- Experiment 4: MDA-MB-231 unmodified, cholesterol depleted, and cholesterol loaded cells were exposed to 0, 0.5, 1.5 MPa peak negative acoustic pressure with $n = 4$.
- Experiment 5: PC3 unmodified, cholesterol depleted, and cholesterol loaded cells were exposed to 0, 0.5, 1.5 MPa peak negative acoustic pressure with $n = 6$.

The data was quantitatively processed with Excel 2003 (Microsoft, USA) and SPSS (IBM, USA). A series of one-way ANOVAs and *post hoc* Tukey statistical tests were applied at 95% confidence interval to analyze the effect of membrane modification on cell permeability and cell viability. Cell permeability and cell viability from each sonoporation experiment were presented as a mean value with standard error bars on 2D plots.

2.5 Therapeutic Ratio

Therapeutic ratio is defined as a ratio of the number of permeabilized and viable cells (FITC-dextran positive and PI negative) to non-viable cells (PI positive). The mean therapeutic ratio for each experiment was calculated.

2.6 Relative Permeability and Relative Viability

Cell permeability from different experiments was compared using a relative permeability parameter. The relative permeability was defined as the ratio of cell permeability of the cholesterol modified samples to the permeability of unmodified samples and was calculated for each peak negative pressure separately. The standard error of the mean was calculated for each pressure and each experiment.

Cell viability from different experiments was compared using a relative viability parameter. It was defined as the ratio of viability of the cholesterol modified samples to the viability of unmodified samples. The standard error of the mean was calculated for each pressure and each experiment.

Chapter 3

Results: Sonoporation of MDA-MB-231 cells

Four experiments were conducted with breast cancer MDA-MB-231 cells with unmodified and cholesterol-modified membranes at two different pressures. The cell permeability results from four experiments are shown on Figure 3.1 and cell viability results from four experiments are shown in Figures 3.2. Cell permeability and viability for each individual experiment are presented and described in Appendix A (Figures A.1-A.4). The corresponding therapeutic ratio from four experiments is plotted on Figure 3.3, while therapeutic ratio from each individual experiment is shown in Appendix A (Figures A.5-A.8). The relative permeability from four experiments is shown on Figure 3.4, while relative permeability at 0.5 and 1.5 MPa for each experiment is shown in Appendix A (Figures A.9 and A.10, respectively). The relative viability from four experiments is plotted on Figure 3.5 and relative viability at 0.5 and 1.5 MPa for each experiment is shown in Appendix A (Figures A.11 and A.12, respectively).

3.1 Cell permeability and cell viability

Cell permeability results from four independent experiments are plotted on Figure 3.1. There is no statistically significant difference in the percentage of permeabilized cells at 0 MPa between unmodified and cholesterol-modified samples. At 0.5 and 1.5 MPa there is no statistically significant differences between unmodified ($15\pm 1.5\%$ and $19\pm 2\%$, respectively) and cholesterol-loaded cells ($12\pm 1.5\%$ and $16\pm 2\%$, respectively), although cholesterol loading leads to decrease in cell permeability at both pressures. On the other hand, permeability of cholesterol-depleted cells ($8\pm 2\%$ and $9\pm 1.5\%$) was statistically lower than that of unmodified ($15\pm 1.5\%$ and $19\pm 2\%$) at 0.5 and 1.5 MPa respectively.

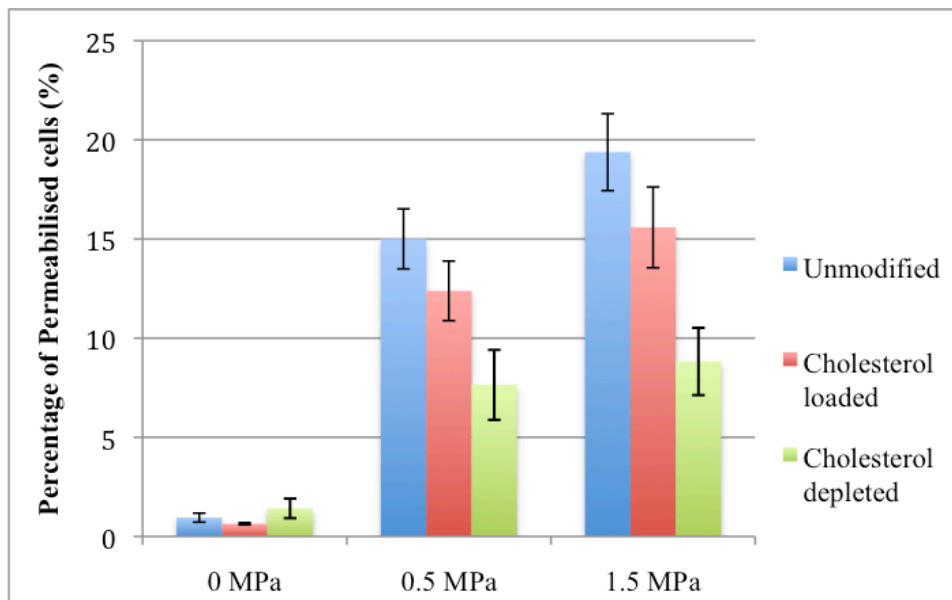


Figure 3.1: The effect of plasma membrane modification with cholesterol loading and depletion on cell permeability of MDA-MB-231 cells from experiments repeated four times.

Cell viability results from four independent experiments are plotted on Figure 2.2. At 0 MPa there is no statistically significant difference in cell viability between unmodified ($87\pm 2\%$), cholesterol-loaded ($85\pm 2\%$), and cholesterol-depleted cells ($84\pm 3\%$). At 0.5 MPa cell viability of cholesterol-depleted cells ($74\pm 5\%$) is the highest and differs significantly from the viability of cholesterol-loaded samples ($57\pm 4\%$). There is no statistically significant difference between cell viability of unmodified ($67\pm 3\%$) and cholesterol-loaded ($57\pm 4\%$) as well as between unmodified ($67\pm 3\%$) and cholesterol-depleted cells ($74\pm 5\%$). At 1.5 MPa no statistically significant difference in cell viability between unmodified ($52\pm 4\%$), cholesterol-loaded ($40\pm 3\%$), and cholesterol-depleted cells ($47\pm 5\%$) was detected.

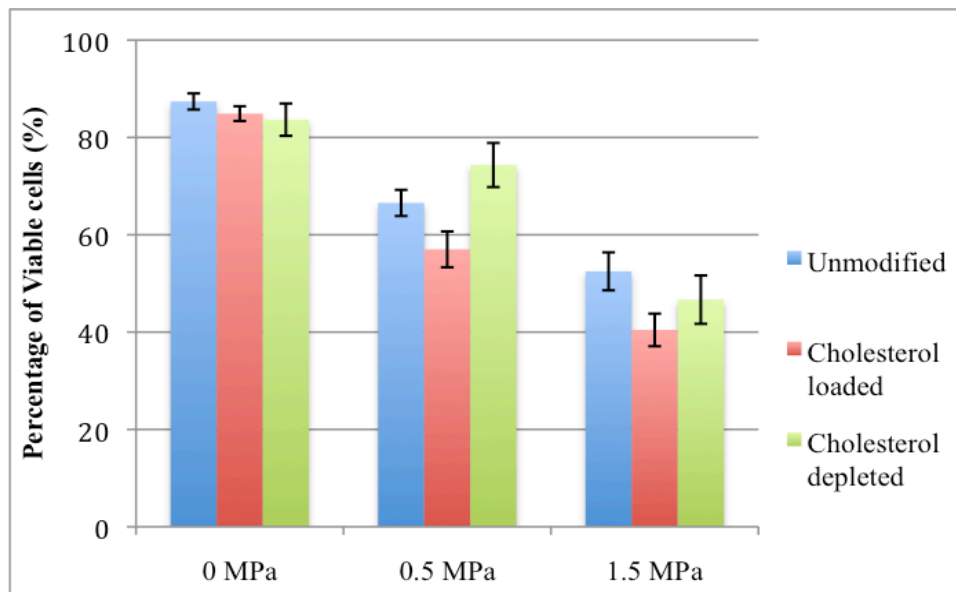


Figure 3.2: The effect of plasma membrane modification with cholesterol loading and depletion on cell viability of MDA-MB-231 cells from experiments repeated four times.

3.2 Therapeutic Ratio

Therapeutic ratio was calculated using cell permeability and cell viability data from four experiments and plotted on Figure 3.3. There is no statistically significant difference in therapeutic ratio between unmodified (0.07 ± 0.01), cholesterol-loaded (0.05 ± 0.01), and cholesterol-depleted MDA-MB-231 cells (0.12 ± 0.04) at 0 MPa. At 0.5 and 1.5 MPa therapeutic ratio of unmodified samples (0.46 ± 0.06 and 0.51 ± 0.08 , respectively) is the highest and differs statistically from the cholesterol-loaded (0.26 ± 0.04 and 0.31 ± 0.06 , respectively) and cholesterol-depleted ones (0.20 ± 0.05 and 0.20 ± 0.04 , respectively).

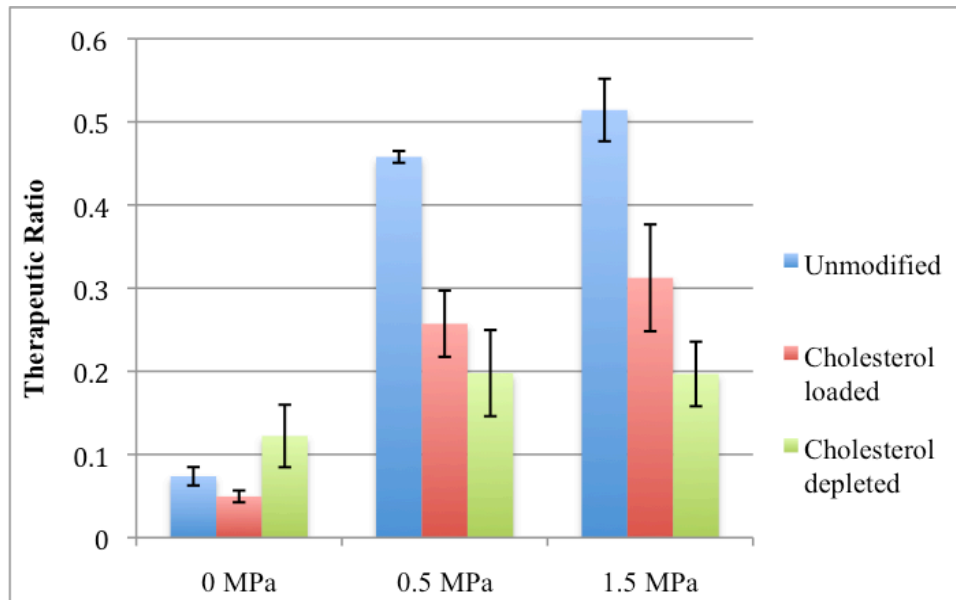


Figure 3.3: The effect of plasma membrane modification with cholesterol loading and depletion on therapeutic ratio of MDA-MB-231 cells from experiments repeated four times.

3.3 Relative Permeability

Figure 3.4 compares the effect of the plasma membrane modification on the mean relative permeability of MDA-MB-231 cells at 0.5 MPa and 1.5 MPa peak negative acoustic pressures from four experiments. The mean relative permeability of cholesterol-depleted cells (0.6 ± 0.1 and 0.37 ± 0.09) differs significantly from the one of unmodified (1 ± 0.1 and 1 ± 0.15) and cholesterol-loaded (0.91 ± 0.11 and 0.83 ± 0.06) cells at 0.5 and 1.5 MPa respectively. At 0.5 and 1.5 MPa there is no statistically significant difference in relative permeability between unmodified (1 ± 0.1 and 1 ± 0.15 , respectively) and cholesterol-loaded (0.91 ± 0.11 , 0.83 ± 0.06) MDA-MB-231 cells.

In general, the alteration of the plasma membrane with cholesterol depletion lowers the relative permeability by 40% and 60% at 0.5 and 1.5 MPa, respectively. Whereas, the cholesterol loading of the cell plasma membrane leads to statistically insignificant decrease in relative permeability, which is more prominent at higher pressure.

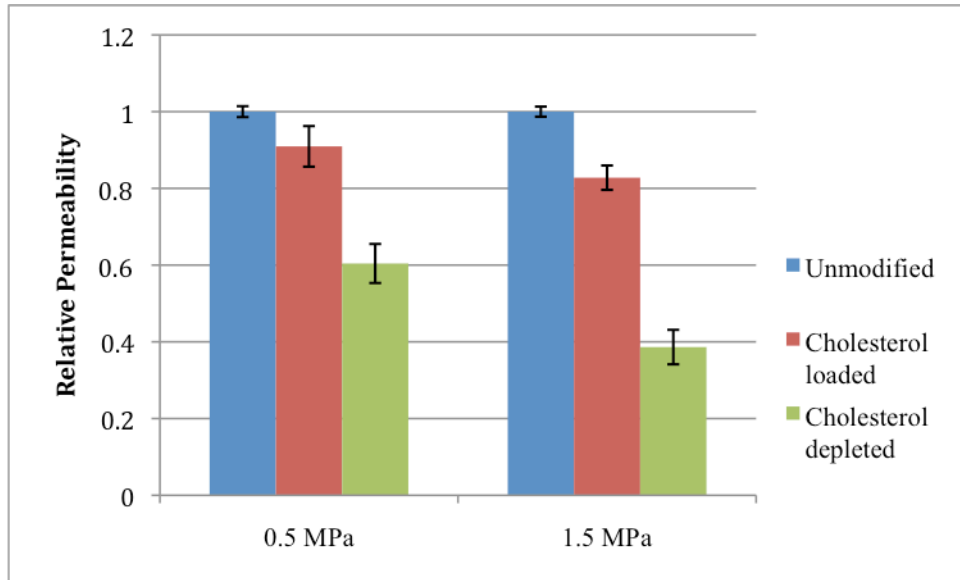


Figure 3.4: The effect of the plasma membrane modification with cholesterol loading and depletion on relative permeability of MDA-MB-231 cells at 0.5 and 1.5 MPa. Each bar represents the average permeability ratio. Error bars represent standard error of the mean within each experiment combined with the standard error across 4 independent experiments for unmodified samples; error bars for cholesterol-loaded and cholesterol-depleted cells represent standard error of the mean within each experiment combined with the standard error across 3 independent experiments.

3.4 Relative viability

The relative viability from four experiments is plotted on Figure 3.5 and relative viability at 0.5 and 1.5 MPa for each experiment is shown on Figures 3A11 and A.12, respectively,

Figure 3.5 compares the effect of the plasma membrane modification on the mean relative viability of MDA-MB-231 cells at 0.5 MPa and 1.5 MPa. At both pressures there is no statistically significant difference in relative viability between unmodified, cholesterol-loaded, and cholesterol-depleted MDA-MB-231 cells.

In conclusion, the alteration of the plasma membrane cholesterol content leads to the statistically insignificant decrease in relative viability, which is more prominent at higher pressure.

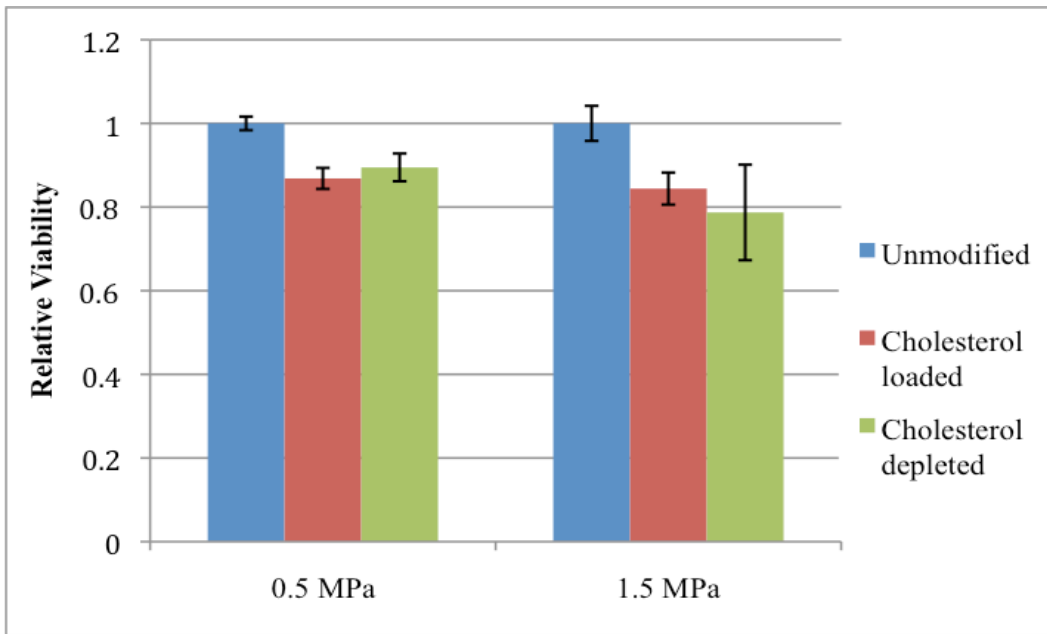


Figure 3.5: The effect of the plasma membrane modification with cholesterol loading and depletion on relative viability of MDA-MB-231 cells at 0.5 and 1.5 MPa. Each bar represents mean relative viability for a given plasma membrane condition (unmodified, cholesterol loaded and cholesterol depleted) and pressure (0.5 and 1.5 MPa). Error bars represent standard error of the mean within each experiment combined with the standard error across 4 independent experiments for unmodified and standard error of the mean within each experiment combined with the standard error across 3 independent for cholesterol loaded and cholesterol depleted cells.

Chapter 4

Discussion

Application of ultrasound in combination with microbubbles has a potential to enhance uptake of normally impermeable molecules and to improve targeted delivery of pharmaceuticals. The cell plasma membrane is considered a primary site of action during the interaction of ultrasound and microbubbles in an *in vitro* cell system. The nature of the interaction appears to be biomechanical based on scanning and transmission electron microscopy images (Deng et al. 2004, Juffermans et al. 2009, Marmottant and Hilgenfeldt 2003). This suggests that the visco-elastic properties of the plasma membrane, such as its fluidity may play a role in the sonoporation process. Fluidity of the plasma membrane is determined in part by the amount of cholesterol present. In this study, it was hypothesized that the change in cholesterol content of the plasma membrane may affect sonoporation process. The cholesterol composition of the plasma membrane was modified with methyl Beta cyclodextrin (M β CD) and cholesterol-loaded M β CD based on a standard protocol. Following membrane modification cells were exposed to ultrasound and microbubbles, and the cell permeability and viability were measured using flow cytometer. The knowledge of the cholesterol's role in the sonoporation process can potentially provide some insight into possible mechanisms of sonoporation and help to identify ways to improve its efficiency in therapeutic applications.

4.1 Sonoporation and Plasma Membrane

The results indicate that there is no simple correlation between cell permeability, cell viability and cholesterol content of the cell plasma membrane. Addition and removal of cholesterol in the cell plasma membrane reduced cell permeability. Cell permeability in cholesterol-loaded MDA-MB-231 cells was lower than in unmodified cells; however, this difference was not statistically significant. Decrease in the cell permeability in cholesterol-depleted MDA-MB-231 cells was observed at 0.5 MPa, but it was not always statistically significant. At 1.5 MPa cell permeability of cholesterol-depleted MDA-MB-231 cells was significantly lower than that of unmodified and cholesterol-loaded cells. However, in experiments with PC3 variation in cell permeability between unmodified and cholesterol-modified samples was insignificant. The highest cell permeability of 30 % was observed at 1.5 MPa peak negative acoustic pressure in unmodified MDA-MB-231 cells. Modification of cell plasma membrane cholesterol content with cholesterol loading and depletion decreases cell viability in both cell lines. However this effect was statistically significant only for experiment 3. The highest cell viability of 77 ± 3 % was observed in unmodified MDA-MB-231 samples in experiment 1 at 0.5 MPa.

The interpretation of the effect of cholesterol modification on the therapeutic ratio – a parameter that was calculated from cell permeability and viability – was challenging due to some variability in cell viability. Variations in the percentage of viable cells, which could have been potentially permeabilized during insonation, may in part explain the large variation in cell permeability across experiments. The difference in cell viability cannot fully account for the variability in cell permeability and most probably there are other factors that play role as well. Therapeutic ratio was the highest in unmodified

MDA-MB-231 samples for both pressures across all experiments. Therapeutic ratio of cholesterol-loaded cells was lower than that of unmodified, although those differences were not always statistically significant. However, therapeutic ratio of cholesterol-depleted MDA-MB-231 cells was always significantly lower than that of unmodified. In PC3 cells the same pattern was observed, but the differences in therapeutic ratio between unmodified and modified cells were not statistically significant.

In order to compare cell permeability across the experiments relative permeability parameter was introduced. It was calculated for each pressure in each experiment separately based on the permeability in unmodified samples. In general, alteration of cell plasma membrane with cholesterol loading leads to the decrease in relative permeability, while cholesterol depletion leads to the significant decrease in relative permeability. This effect was more prominent at higher pressure in MDA-MB-231 cells. Differences in relative permeability parameter in between unmodified and cholesterol-modified samples agree well with cell permeability statistical differences in between unmodified and cholesterol-modified samples. Therefore, relative permeability is a suitable parameter to compare cell permeabilization across independent experiments.

To compare cell viability across the experiments a relative viability parameter was used. It was shown that the alteration of the plasma membrane cholesterol content lead to a slight decrease in relative viability in MDA-MB-231 cells for the majority of the conditions. This decrease is more prominent at higher pressure, and was not observed in PC3 cells.

Moreover, with increase in peak negative acoustic pressure cell permeability increase and viability decrease in both cell lines, which correlates with results by

Karshafian et al. (2009). Comparing the sonoporation outcome between the two cell lines it was observed that the MDA-MB-231 were more permeable to FITC-dextran than the PC3 cells, at all pressures, which may be attributed to differences in their plasma membrane composition.

Since the incubation time and the concentration of M β CD and cholesterol-M β CD used was the same as used by Goodwin et al. (2005) and Lagerholm et al. (2005) it was assumed that the cholesterol level of the cell plasma membranes in this study was reduced by 50% and increased by 300%. Changes in cholesterol concentration in the plasma membrane affects membrane fluidity (Lars Bastiaanse et al. 1997), permeability to small molecules (Klein et al. 1995), and certain types of endocytosis (Cossec et al. 2010, Rodal et al. 1999). Although, the cholesterol content was not measured following depletion and loading, it is believed that the modification was significant and its quantification will be a subject for future investigations. The non-uniform distribution of cholesterol across the cell plasma membrane and the presence of lipid domains make the accurate measurement of cholesterol content challenging. Illangumaran and Hoessli (1998) hypothesized that M β CD extracts only the cholesterol tightly associated with glycerophospholipids, while the cholesterol in sphingolipids rich regions become resistant to M β CD. Two cell lines that were used in current study originated from different organs (MDA-MB-231 is the breast cancer, PC3 is the prostate cancer); therefore it is possible that the ratio of glycerophospholipids to sphingolipids is different in those two cell lines. However, no scientific confirmation to that was found. If it is true, then the amount of cholesterol extracted and loaded may be different for MDA-MB-231 and PC3, which would have to be confirmed by quantitative measurement.

A search of relevant literature found no studies on the effect of cholesterol content on sonoporation process. However, the decrease in cell permeability of cholesterol-loaded MDA-MB-231 cells may be partially supported by the studies on pore formation through electroporation. Koronkiewicz and Kalinowski (2004) performed constant-current measurements of egg yolk phosphatidylcholine bilayer membrane without and with cholesterol. They observed poration facilitated by constant-intensity current flow. The presence of cholesterol in the membrane required higher value of the breakdown potential compare to the control. They concluded that the presence of cholesterol makes membranes more resistant to pore formation. Kakorin et al. (2005) observed reduction in membrane electroporation facilitated by cholesterol in lipid vesicles. However, it must be taken into consideration that the process of pore formation in electroporation and sonoporation is different and the cell plasma membrane is more complicated structure than egg yolk phosphatidylcholine bilayer or lipid vesicles. Decrease in permeability of cholesterol-depleted cells cannot be explained by known studies and should be a subject of further research.

Multiple studies were conducted on the effect of plasma membrane fluidity on electroporation. The cholesterol content of plasma membrane is directly linked to the membrane fluidity: lowering of cholesterol content makes the membrane more fluid and vice versa (Lars Bastiaanse et al. 1997). The study by Kanduser et al. (2006) conducted on different cell lines demonstrated that less fluid cells were permeabilized at lower voltages compare to more fluid cells. The modification of fluidity with temperature confirmed the above statement: less fluid membranes had a higher electro-permeabilization (Kanduser et al. 2008). In contrast, the modification of fluidity with

ethanol and lysolecitin showed that less fluid membranes were permeabilized at higher voltage (Rolls et al. 1990).

It was demonstrated that addition of cholesterol to the cell plasma membrane altered the physical state of the membrane, which affected the function of integral proteins (Gleason et al. 1991). For example, an increase in plasma membrane cholesterol was correlated with decrease in activities of adenylate cyclase (Whetton et al. 1983), Na⁺, K⁺, -ATPase (Schwarz et al. 1988), and alkaline phosphatase

In addition, cholesterol concentration affects clathrin-mediated endocytosis (Rodal et al. 1999). Over a wide range of cholesterol concentrations from -40% to +40%, modified with M β CD and cholesterol-loaded M β CD, Cossec et al. (2010) demonstrated a dose-dependent and linear relationship between cholesterol concentration in plasma membrane and clathrin-dependent endocytosis. They suggested that an excess of cholesterol in the plasma membrane accelerates this type of endocytosis. However, the role of endocytosis in sonoporation is still debatable. It is believed that bigger molecules (155-500 kDa) are more likely to enter the cell via endocytosis, while smaller molecules (up to 70 kDa) are more likely to enter the cell via pore formation (Meijering et al. 2009). In current study we used FITC-dextran whose size is 70 kDa, which based on the above assumption should enter the cells through the pores. This explains the absence of increase in permeabilization of cholesterol-loaded cells. Testing the uptake of bigger molecules by unmodified, cholesterol-loaded and depleted cells should be part of future studies.

4.2 Limitations of this study

There are a number of limitations to the current study. The results show a lack of consistency in cell permeability through the experiments with MDA-MB-231 cells. Permeability ratio parameter was introduced to run the comparison in between cell permeability across experiments. The statistically significant differences in permeability ratio agree well with differences in cell permeability. Therefore, the introduction of permeability ratio parameter is fully justifiable for the sake of comparison of sonoporation outcome across independent experiments.

The four experiments with MDA-MB-231 cells were conducted during a time span of three months. It is probable that the cells underwent certain physiological modifications related to regular trypsinization. Doing experiments with cells originating from the same flask and with a minimal time intervals in between may help to achieve more consistent result. Secondly, careful standardization of the biological procedures such as regular cells maintenance, sample preparation, cells count, and addition of membrane modifying agents, as well as dyes, is required. Thirdly, the way the data was analyzed with fluorescent markers and flow cytometry may have introduced some level of uncertainty into our results. The fluorescence emission spectra of FITC-dextran and PI overlap, which should be corrected with fluorescence compensation.

The *in vitro* cell suspension model used in the experiments allows considerable control of environmental, biological, and exposure parameters. However, it may not mirror the results from an *in vivo* model. To increase the relevance of *in vitro* studies to *in vivo* ones careful standardization of acoustical and biological experimental procedures is necessary.

The exposure chamber, where the cell samples were positioned during insonation, has round acoustically transparent windows that do not cover the entire chamber wall. Therefore, approximately 70% of cells suspension was insonated at maximum acoustic pressure based on the chamber geometry. This limitation was partially corrected with the presence of magnetic stirrer underneath the chamber, which gently mixed cell suspension during insonation.

The experiments were conducted at room temperature ($\sim 22^{\circ}\text{C}$) because a lot of time-consuming cell preparatory work was done inside the biological hood, which cannot be heated to 37°C . To make the results more biologically relevant all the experimental procedures have to be performed at 37°C .

In addition, we measured sonoporation outcome based on the cell permeability and cell viability, which cannot evaluate the ability of insonated cells to proliferate. Clonogenic viability describes the cells ability to proliferate following exposure to ultrasound and microbubbles and will be measured in a future work.

Chapter 5

Conclusions and future work

5.1 Conclusions

In conclusion, our results indicate that modification of the cholesterol content in the cell plasma membrane affects ultrasound and microbubbles induced cell permeabilization in an *in vitro* cell suspension model. MDA-MB cells with cholesterol-depleted plasma membrane were less permeable to FITC-dextran molecules compare to unmodified and cholesterol-loaded cells. This effect depended on the peak negative acoustic pressure and cell type as well. Understanding the role of cholesterol in plasma membrane during ultrasound and microbubble permeabilization may provide more insight into the sonoporation process and help to improve intracellular drug delivery applications.

5.2 Future Work

Improving our understanding of sonoporation requires studies to be conducted on the effects of cell biomechanical properties, such as plasma membrane fluidity and cytoskeleton composition. This study demonstrated that cholesterol plays a role in sonoporation. Future studies should quantitatively investigate the correlation between cholesterol content and cell permeability by measuring the cholesterol content of the

plasma membrane following depletion and loading of cholesterol. In addition, this study showed that ultrasound peak negative pressure is important. Future work should measure sonoporation outcome for a wider range of pressures, which may provide more insight on the combined effect of membrane cholesterol concentration and acoustic pressure. Furthermore, Juffermans et al. 2009 looked at the rearrangement of actin filaments following ultrasound and microbubbles exposure in cells with natural cholesterol content. Modifying cell plasma membrane cholesterol content and repeating the above work may provide linkage between cholesterol and actin concentrations, and sonoporation efficiency.

In addition, cells with different cholesterol content in plasma membranes can be used to investigate the effect of membrane cholesterol on sonoporation process. One set of experiments was conducted with prostate cancer (PC3) cells. However, to make the results more conclusive those experiments should be repeated and the difference in membrane cholesterol content between breast and prostate cancer cells should be quantified.

5.2.1 Sonoporation of PC3 cells

One experiment ($n=6$) was conducted with prostate cancer (PC3) cells with unmodified and cholesterol-modified membranes at two different pressures. The cell permeability is shown on Figure 5.1 and cell viability is shown on Figure 5.2. Therapeutic ratio is shown on Figure 5.3. Relative permeability at 0.5 and 1.5 MPa is shown on Figure 5.4. Relative viability at 0.5 and 1.5 MPa is shown on Figure 5.5.

Cell permeability and cell viability

Figure 5.1 represents cell permeability of PC3 cells from one experiment (Experiment 5). Cell permeability of unmodified cells ($7\pm 1\%$ and $9\pm 2\%$) at 0.5 and 1.5 MPa is not statistically different from that of cholesterol-loaded ($4\pm 1\%$ and $9\pm 2\%$) and cholesterol-depleted ($4\pm 1\%$ and $8\pm 1\%$). The maximum percentage of permeabilized PC3 cells - 9% was observed at 1.5 MPa in unmodified samples. Overall, the percentage of permeabilized PC3 cells was lower than that of MDA-MB-231 cells from four experiments (Figures 3.1)

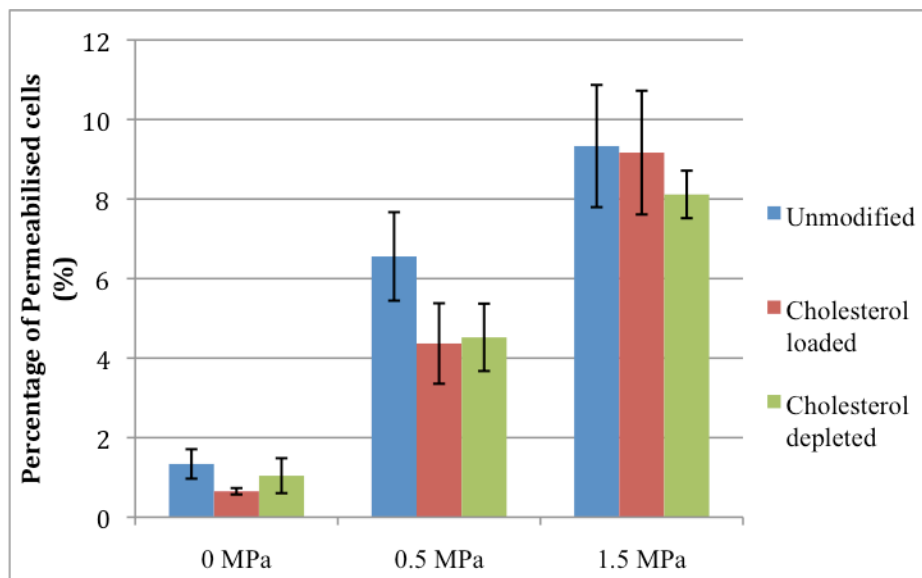


Figure 5.1: The effect of the plasma membrane modification with cholesterol loading and depletion and peak negative pressure on cell permeability of PC3 in experiment 5 ($n=6$). The percentage of permeabilized and viable cells are shown with respect to peak negative acoustic pressure, where P is the number of permeabilized cells which remain viable and V is the number of viable cells.

Figure 5.2 represents cell viability of PC3 cells. Viability of unmodified ($72\pm 3\%$ and $64\pm 3\%$ at 0.5 and 1.5 MPa respectively) PC3 cells was not statistically different from

the viability of cholesterol-loaded ($69\pm 2\%$ and $64\pm 4\%$ at 0.5 and 1.5 MPa respectively), and cholesterol-depleted ($73\pm 3\%$ and $66\pm 5\%$ at 0.5 and 1.5 MPa respectively).

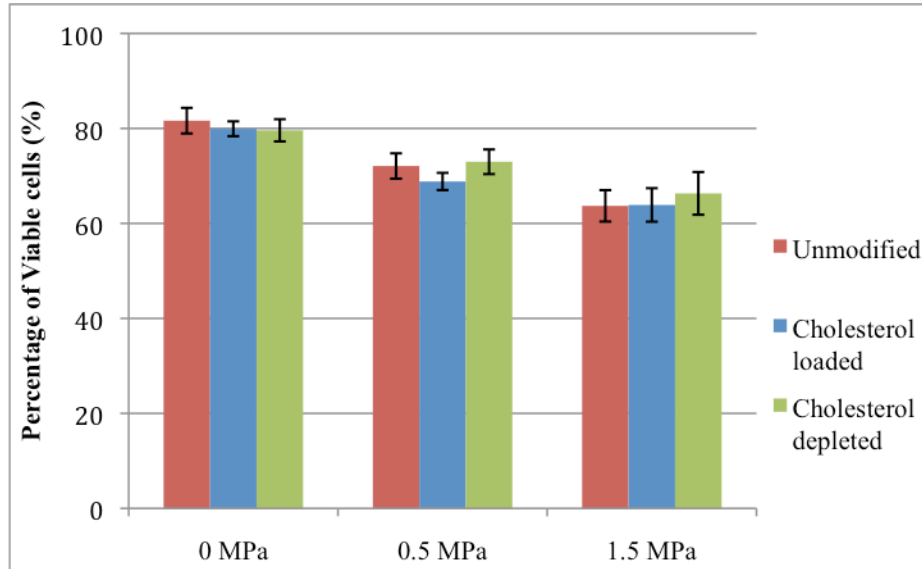


Figure 5.2: The effect of the plasma membrane modification with cholesterol loading and depletion and peak negative pressure on cell viability of PC3 in experiment 5 ($n=6$). The percentage of permeabilized and viable cells are shown with respect to peak negative acoustic pressure, where P is the number of permeabilized cells which remain viable and V is the number of viable cells.

Therapeutic Ratio

The therapeutic ratio is calculated using cell permeability and cell viability data from experiment 5 is shown on Figure 5.3. Therapeutic ratio of unmodified (0.24 ± 0.05) PC3 cells was slightly higher than that of cholesterol-loaded (0.14 ± 0.04) and cholesterol-depleted (0.16 ± 0.03) cells at 0.5 MPa; however, this difference is not statistically significant, which agrees with the cell permeability and the cell viability results. At 1.5 MPa there was no statistically significant difference in therapeutic ratio of unmodified (0.26 ± 0.05), cholesterol-loaded (0.27 ± 0.04), and cholesterol-depleted (0.28 ± 0.04) PC3 cells as well, which agrees with the cell permeability and the cell viability data. The value

for therapeutic ratio of unmodified PC3 cells (0.24 ± 0.05) lies in a range of values, obtained from MDA-MB-231 experiments (from 1.13 ± 0.09 to 0.2 ± 0.08). Therapeutic ratio of cholesterol-loaded PC3 (0.14 ± 0.04) agrees with that obtained from experiments 1-4 with MDA-MB-231 (from 0.73 ± 0.04 to 0.13 ± 0.01). Finally, therapeutic ratio of cholesterol-depleted PC3 cells (0.16 ± 0.03) is in a range of values from experiments with MDA-MB-231 cells (from 0.33 ± 0.03 to 0.03 ± 0.01).

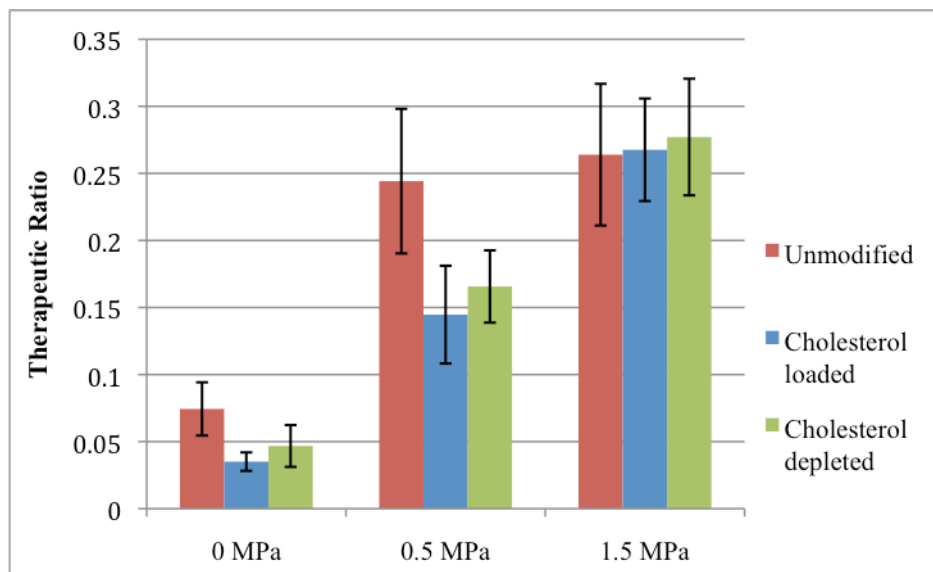


Figure 5.3: The effect of the plasma membrane modification with cholesterol loading and depletion and peak negative pressure on the therapeutic ratio of PC3 in experiment 5 ($n = 6$). The y-axis represents the therapeutic ratio; the x-axis represents peak negative acoustic pressure in MPa.

Relative Permeability

Figure 5.5 compares the effect of the plasma membrane modification on relative permeability of PC3 cells at 0.5 MPa and 1.5 MPa. At 0.5 MPa there is statistically significant difference in relative permeability between unmodified (1 ± 0.14) and cholesterol-loaded (0.67 ± 0.14), between unmodified (1 ± 0.14) and cholesterol-depleted (0.68 ± 0.12) PC3 cells. Similar decrease in permeability of was observed in cholesterol-

modified cells, compared to unmodified; however it was not statistically significant. In addition, there was no statistically significant difference in relative permeability between cholesterol-loaded (0.67 ± 0.14) and cholesterol-depleted (0.68 ± 0.12) cells, which agrees with the cell permeability data from PC3 as well as from MDA-MB-231 samples. At 1.5 MPa there is no statistically significant difference in relative permeability between unmodified (1 ± 0.22), cholesterol-loaded, (1 ± 0.22) and cholesterol-depleted (0.89 ± 0.11) cells. Same tendency was observed with cell permeability.

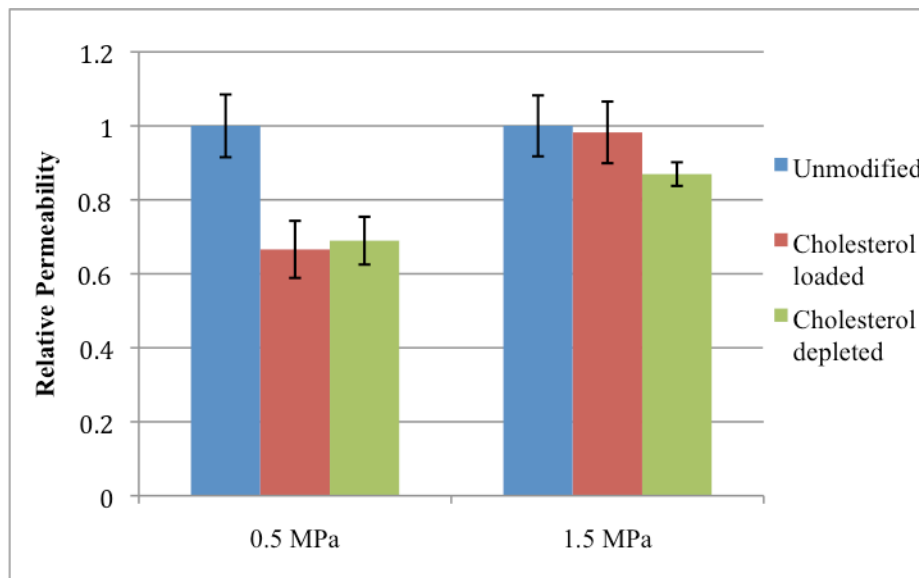


Figure 5.4: The effect of the peak negative pressure and the plasma membrane modification with cholesterol loading and depletion on relative permeability of PC3 cells in Experiment #5. Each bar represents mean relative permeability for a given plasma membrane condition (unmodified, cholesterol loaded and cholesterol depleted) and pressures (0.5 and 1.5 MPa) from one experiment. Error bars represent standard error of the mean for $n = 6$.

Relative Viability

Figure 5.5 compares the effect of the plasma membrane modification on relative viability of PC3 cells at 0.5 MPa and 1.5 MPa. At 0.5 and 1.5 MPa there is no statistically significant difference in relative viability between unmodified (1 ± 0.04 and 1 ± 0.05 ,

respectively), cholesterol-loaded (0.96 ± 0.03 and 1 ± 0.06 , respectively), and cholesterol-depleted (1.01 ± 0.04 and 1.03 ± 0.08 , respectively) MDA-MB-231 cells. This agrees with the cell viability data.

In conclusion, alteration of the plasma membrane cholesterol content results in no statistically significant difference in relative viability, as well as viability at 0.5 and 1.5 MPa.

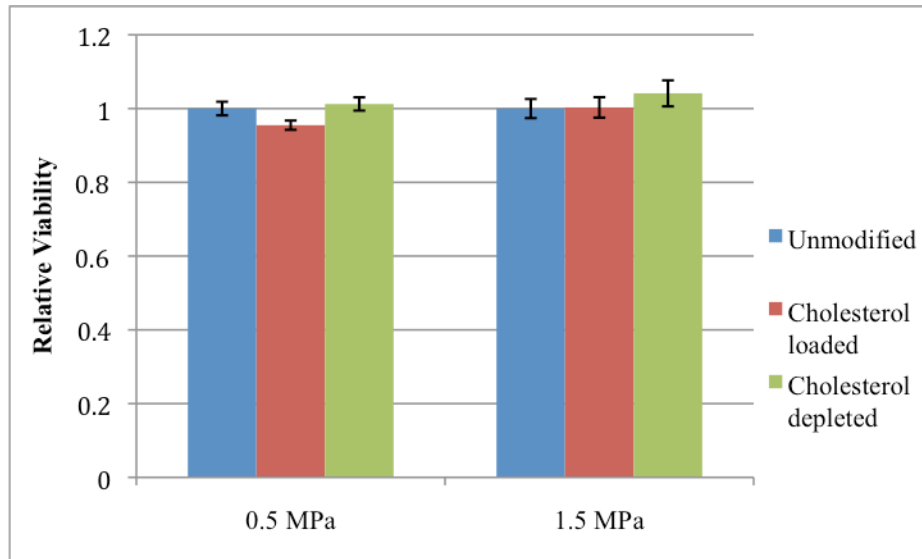


Figure 5.5: The effect of the peak negative pressure and the plasma membrane modification with cholesterol loading and depletion on relative viability of PC3 cells in Experiment #5. Each bar represents mean relative viability for a given plasma membrane condition (unmodified, cholesterol loaded and cholesterol depleted) and pressure (0.5 and 1.5 MPa). Error bars represent standard error of the mean for $n = 6$.

5.2.2 Measuring cholesterol content of cell plasma membrane

To obtain the correlation between cell permeability and cholesterol loading and depletion the cholesterol content of cell plasma membrane should be measured. Illangumaran and Hoessli (1998) evaluated cholesterol content of lymphocytes and endothelial cells by peleting and extraction of total plasma membranes with chloroform/methanol. Another method to detect and quantify cholesterol in the membranes is treatment with filipin, a fluorescent polyene antibiotic (Tallima and Ridi 2005), which binds to unesterified 3β -hydroxy-sterols.

Appendix A

A.1 Cell permeability and cell viability of MDA-MB-231 cells

The results from experiments 1-4 demonstrated that the cell permeability of unmodified MDA-MB-231 cells is higher compared to the permeability of cells with modified plasma membrane cholesterol content (Figure A.1, A.2, A.3, and A.4). Furthermore, the permeability of cholesterol-loaded cells on average is higher compared to the permeability of the cholesterol-depleted cells.

In experiment 1 (Figure A.1) cell permeability of unmodified cells ($20\pm 2\%$) is statistically higher compared to the permeability of cholesterol-depleted cells ($9\pm 0.5\%$) at 1.5 MPa. However, at 0.5 MPa, no statistically significant differences were measured between unmodified ($18\pm 3\%$) and cholesterol-depleted cells ($13\pm 2\%$). The maximum permeability of unmodified cells ($20\pm 2\%$) was achieved at 1.5 MPa compared to the maximum permeability of cholesterol-depleted cells ($13\pm 2\%$), measured at 0.5 MPa. In addition, no statistically significant differences were observed in cell viability between unmodified and cholesterol-depleted cells at both pressures.

In experiment 2 (Figure A.2) no statistically significant difference is observed between unmodified ($18\pm 1\%$ and $18\pm 2\%$ at 0.5 and 1.5 MPa, respectively) and cholesterol-loaded ($15\pm 1\%$ and $13\pm 1\%$ at 0.5 and 1.5 MPa, respectively) cells. The percentages of permeabilized cells in unmodified samples at both pressures are comparable to the ones, measured in unmodified samples in experiments 1 (Figure A.1). In addition, no statistically significant difference was measured in cell viability, assessed with PI, between unmodified and cholesterol-loaded cells at 0.5 and 1.5 MPa.

In experiment 3 (Figure A.3) no statistically significant difference in cell permeability is observed between unmodified ($31\pm 5\%$) and cholesterol-loaded ($28\pm 1\%$) cells at 1.5 MPa. This result agrees with experiment 2 data (Figure A.2). A statistically significant difference in cell permeability was measured between unmodified ($31\pm 5\%$) and cholesterol-depleted ($15\pm 2\%$) cells. This result agreed with experiment 1 (Figure A.1). Furthermore, a statistically significant difference in cell permeability was observed between cholesterol-depleted ($15\pm 2\%$) and cholesterol-loaded ($28\pm 1\%$) cells at 1.5 MPa. However, higher cell permeability in unmodified samples was achieved in experiment 3 ($31\pm 5\%$) compared to experiments 1 ($20\pm 2\%$), 2 ($18\pm 2\%$) and 4 ($10\pm 2\%$). There is statistically significant difference in cell viability between unmodified ($73\pm 3\%$) and cholesterol-loaded ($61\pm 1\%$), between unmodified ($73\pm 3\%$) and cholesterol-depleted ($41\pm 4\%$) cells, and between cholesterol-loaded and cholesterol-depleted, which disagreed with experiments 1 and 2.

In experiment 4 (Figure A.4) no statistically significant difference in cell permeability is observed between unmodified ($7\pm 1\%$ and $10\pm 2\%$ for 0.5 and 1.5 MPa, respectively) and cholesterol-loaded cells ($7\pm 1\%$ and $8\pm 1\%$ for 0.5 and 1.5 MPa, respectively). This observation agrees with all the previous experiments. A statistically significant difference was observed between unmodified ($7\pm 1\%$ and $10\pm 2\%$ for 0.5 and 1.5 MPa, respectively) and cholesterol-depleted ($3\pm 0.1\%$ and $2\pm 0.1\%$ for 0.5 and 1.5 MPa, respectively) and between cholesterol-loaded ($7\pm 1\%$ and $8\pm 1\%$ for 0.5 and 1.5 MPa, respectively) and cholesterol-depleted ($3\pm 0.1\%$ and $2\pm 0.1\%$ for 0.5 and 1.5 MP, respectively). This observation agreed with all experiments. However, the lowest cell permeability in unmodified cells – $7\pm 1\%$ and $10\pm 2\%$ at 0.5 and 1.5 MPa, respectively –

was achieved in experiment 4 (Figure A.4). In experiment 4, there is no statistically significant difference in cell viability between unmodified and modified cells at both pressures, which agrees with results from experiment 1 (Figure A.1) and 2 (Figure A.2) and disagrees with results from experiment 3 (Figure A.3).

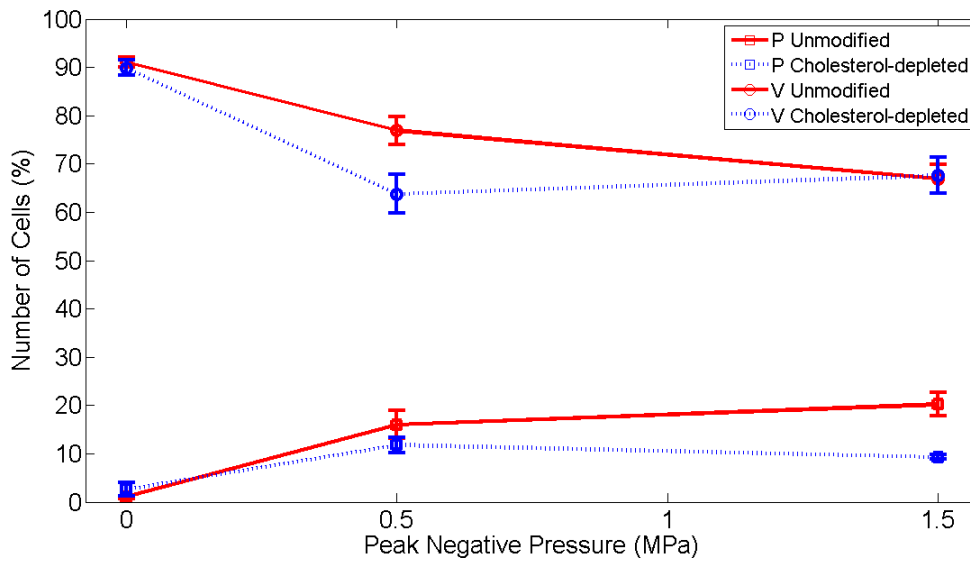


Figure A.1: The effect of the plasma membrane modification with cholesterol depletion and peak negative pressure on cell permeability and cell viability of MDA-MB-231 in experiment 1 ($n=4$). The percentage of permeabilized and viable cells are shown with respect to peak negative acoustic pressure, where P is the number of permeabilized cells which remain viable and V is the number of viable cells.

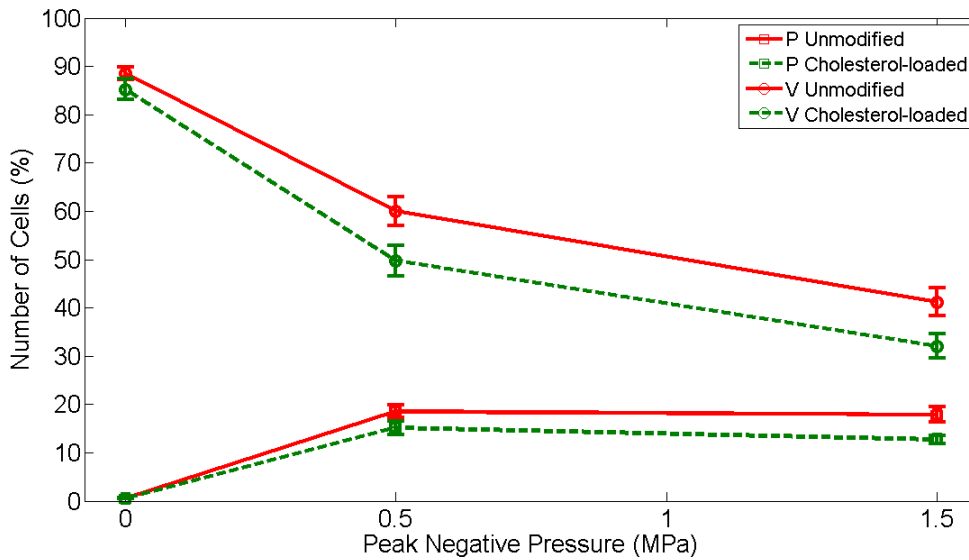


Figure A.2: The effect of the plasma membrane modification with cholesterol loading and peak negative pressure on cell permeability and cell viability of MDA-MB-231 in experiment 2 ($n=8$). The percentage of permeabilized and viable cells are shown with respect to peak negative acoustic pressure, where P is the number of permeabilized cells which remain viable and V is the number of viable cells.

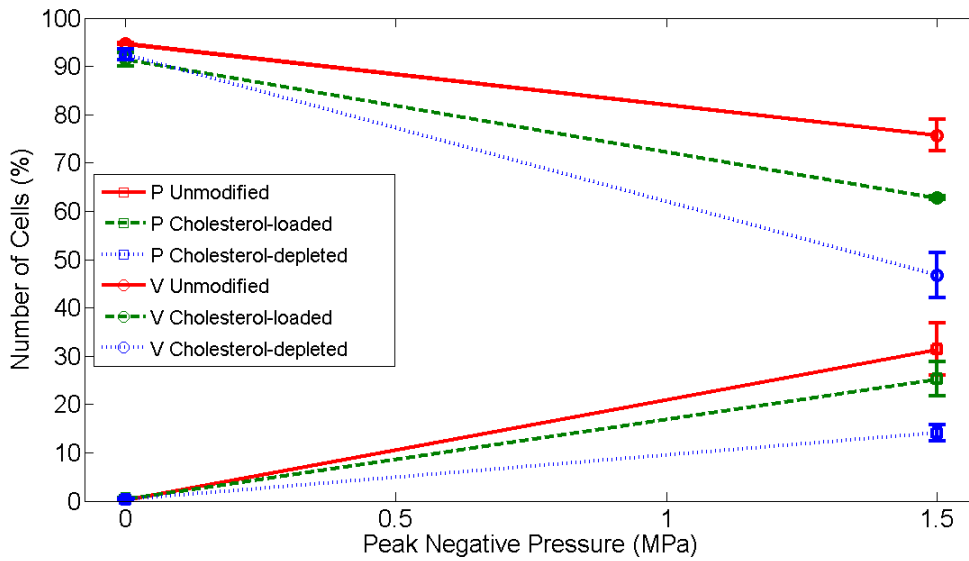


Figure A.3: The effect of the plasma membrane modification with cholesterol loading and depletion and peak negative pressure on cell permeability and cell viability of MDA-MB-231 in experiment 3 ($n=4$). The percentage of permeabilized and viable cells are shown with respect to peak negative acoustic pressure, where P is the number of permeabilized cells which remain viable and V is the number of viable cells.

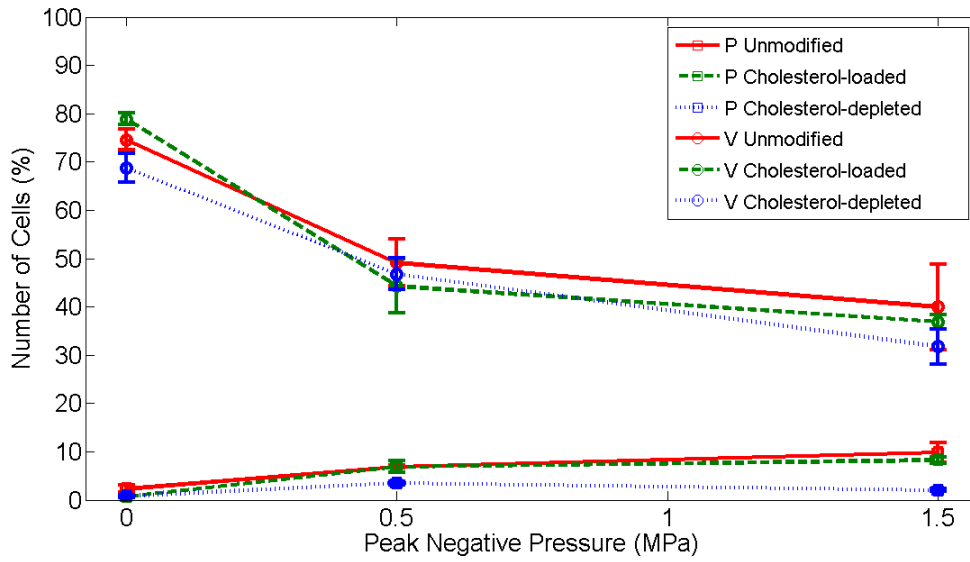


Figure A.4: The effect of the plasma membrane modification with cholesterol loading and depletion and peak negative pressure on cell permeability and cell viability of MDA-MB-231 in experiment 4 ($n=4$). The percentage of permeabilized and viable cells are shown with respect to peak negative acoustic pressure, where P is the number of permeabilized cells which remain viable and V is the number of viable cells.

A.2 Therapeutic Ratio of MDA-MB-231 cells

The therapeutic ratio calculated using cell permeability and cell viability data from experiments 1 - 4 is shown in Figures A.5, A.6, A.7, and A.8. Higher therapeutic ratio is achieved with unmodified cells (ranging from 1.13 ± 0.09 to 0.2 ± 0.08) compared to cholesterol-depleted (ranging from 0.33 ± 0.03 to 0.03 ± 0.01) and cholesterol-loaded (ranging from 0.73 ± 0.04 to 0.13 ± 0.01) MDA-MB-231 cells.

In experiment 1 (Figure A.5) at 0.5 and 1.5 MPa there is statistically significant difference in therapeutic ratio between unmodified (0.70 ± 0.12 and 0.61 ± 0.03 , respectively) and cholesterol-depleted MDA-MB-231 cells (0.33 ± 0.03 and 0.29 ± 0.03 , respectively). Significant difference between unmodified and cholesterol-depleted samples was observed in cell permeability at 1.5 MPa (Figure A.1). However, there is no statistically significant difference between unmodified and cholesterol-depleted samples in cell permeability at 0.5 MPa and in cell viability at both pressures.

In experiment 2 (Figure A.6) at 0.5 and 1.5 MPa there is no statistically significant difference in therapeutic ratio between unmodified (0.5 ± 0.07 and 0.33 ± 0.05 for 0.5 and 1.5 MPa respectively) and cholesterol-loaded MDA-MB-231 cells (0.32 ± 0.05 and 0.19 ± 0.02 for 0.5 and 1.5 MPa respectively). The difference in cell permeability and cell viability between unmodified and cholesterol-loaded MBA-MB-231 cells were statistically insignificant as well (Figure A.2).

In experiment 3 (Figure A.7) at 1.5 MPa there is statistically significant difference in therapeutic ratio between unmodified (1.13 ± 0.09) and cholesterol-depleted (0.26 ± 0.04) cells, which agrees with the results from experiment 1. There is statistically significant difference in cell permeability and cell viability between unmodified and cholesterol-

depleted cells (Figure A.3). There is statistically significant difference in therapeutic ratio between unmodified (1.13 ± 0.09) and cholesterol-loaded cells (0.73 ± 0.04), which disagrees with the results from experiment 2. There is no statistically significant difference in cell permeability between unmodified and cholesterol-loaded cells, but there is a significant difference in cell viability between them. In addition, there is statistically significant difference in therapeutic ratio between cholesterol-loaded (0.73 ± 0.04) and cholesterol-depleted (0.26 ± 0.04) MDA-MB-231 cells. This statistically significant difference was present in cell permeability and cell viability as well.

In experiment 4 (Figure A.8) at 0.5 and 1.5 MPa there is statistically significant difference in therapeutic ratio between unmodified (0.14 ± 0.01 and 0.2 ± 0.08 at 0.5 and 1.5 MPa respectively) and cholesterol-depleted cells (0.07 ± 0.01 and 0.03 ± 0.01 at 0.5 and 1.5 MPa respectively), which agrees with the results from experiment 1 and 3. Moreover, there is statistically significant difference in cell permeability, but not in cell viability between unmodified and cholesterol-depleted cells (Figure A.4). There is no significant difference in therapeutic ratio at 0.5 and 1.5 MPa between unmodified (0.14 ± 0.01 and 0.2 ± 0.08 at 0.5 and 1.5 MPa respectively) and cholesterol-loaded cells (0.13 ± 0.04 and 0.13 ± 0.01), which agrees with the results from experiment 2, but disagrees with the results from experiment 3 at 1.5 MPa. There is no statistically significant difference in cell permeability and cell viability between unmodified and cholesterol-loaded MDA-MB-231 cells at both pressures.

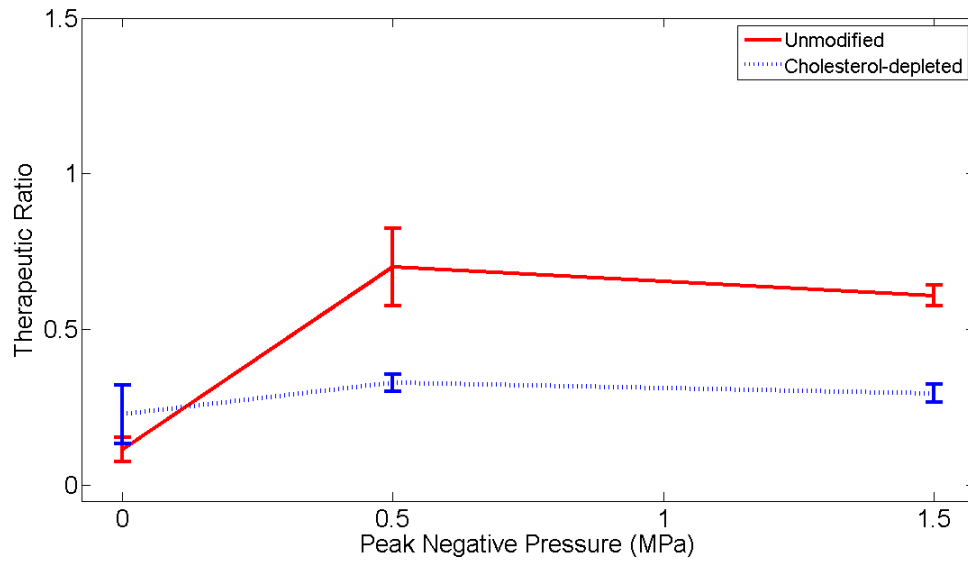


Figure A.5: The effect of the plasma membrane modification with cholesterol depletion and peak negative pressure on the therapeutic ratio of MDA-MB-231 in experiment 1 ($n=4$). The y -axis represents the therapeutic ratio; the x -axis represents peak negative acoustic pressure in MPa.

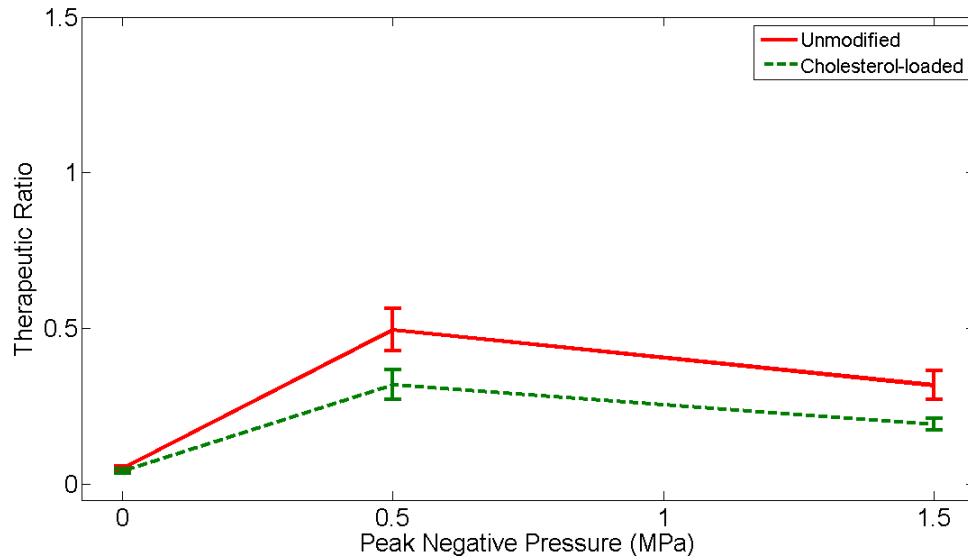


Figure A.6: The effect of the plasma membrane modification with cholesterol loading and peak negative pressure on the therapeutic ratio of MDA-MB-231 in experiment 2 ($n=8$). The y -axis represents the therapeutic ratio; the x -axis represents peak negative acoustic pressure in MPa.

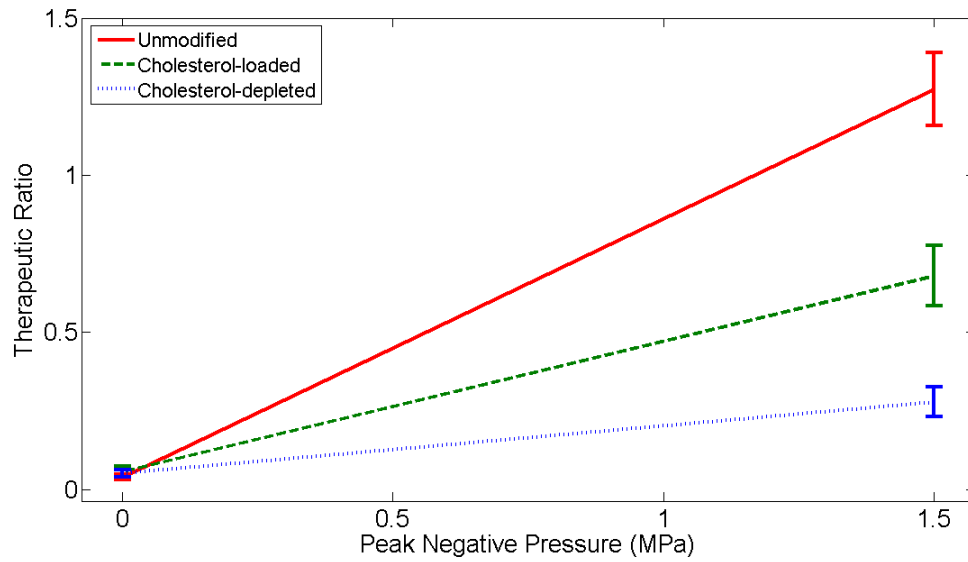


Figure A.7: The effect of the plasma membrane modification with cholesterol loading and depletion and peak negative pressure on the therapeutic ratio of MDA-MB-231 in experiment 3 ($n=4$). The y -axis represents the therapeutic ratio; the x -axis represents peak negative acoustic pressure in MPa.

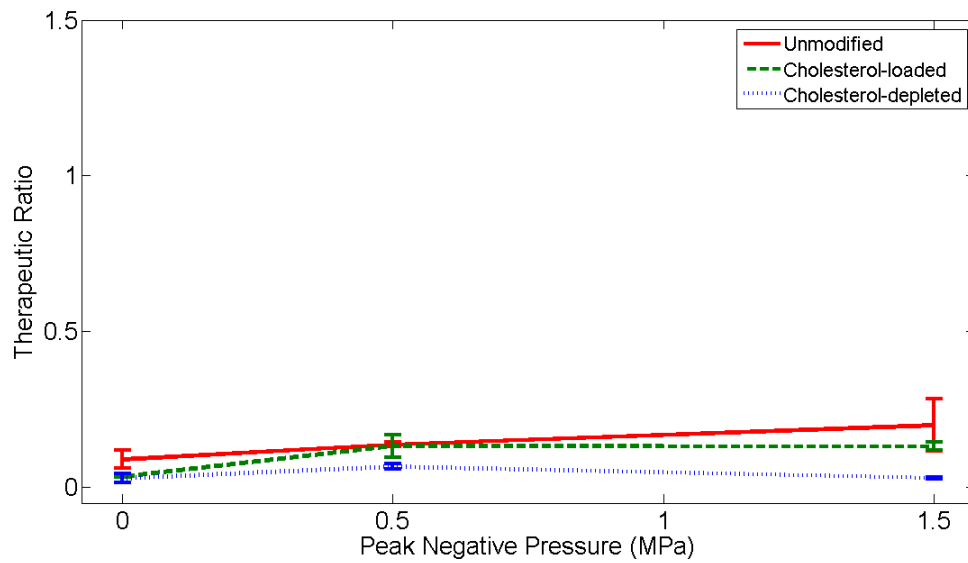


Figure A.8: The effect of the plasma membrane modification with cholesterol loading and depletion and peak negative pressure on the therapeutic ratio of MDA-MB-231 in experiment 4 ($n=4$). The y -axis represents the therapeutic ratio; the x -axis represents peak negative acoustic pressure in MPa.

A.3 Relative Permeability of MDA-MB-231 cells

The relative permeability for each experiment conducted at 0.5 MPa and 1.5 MPa are shown in Figures A.9 and A.10, respectively.

Relative permeability for each experiment

Experiment 1: The permeability ratio of unmodified MDA-MB-231 cells (1 ± 0.17) exposed to 0.5 MPa acoustic pressure is lower, but not statistically different (on 95% confidence interval) from the permeability ratio of cholesterol-depleted cells (0.72 ± 0.11) (Figure A.9). This agrees well with the cell permeability results. At 1.5 MPa, a statistically significant difference was observed in permeability ratio between unmodified (1 ± 0.12) and cholesterol-depleted (0.45 ± 0.02) MDA-MB-231 cells on 95% confidence interval. Similar statistically significant decrease was observed in cell permeability (Figure A.1).

Experiment 2: At 0.5 and 1.5 MPa the permeability ratio of cholesterol-loaded cells (0.83 ± 0.06 and 0.72 ± 0.06 at 0.5 and 1.5 MPa respectively) is lower than that of unmodified cells (1 ± 0.06 and 1 ± 0.11 at 0.5 and 1.5 MPa respectively), however the difference was not statistically significant, which agrees with the cell permeability results (Figure A.2).

Experiment 3: At 1.5 MPa there is no statistically significant difference in permeability ratio between unmodified (1 ± 0.16) and cholesterol-loaded (0.90 ± 0.03) MDA-MB-231 cells, which agrees with the cell permeability data (Figures A.3) and permeability ratio results from experiment 2. At the same time permeability ratio of cholesterol-depleted cells (0.48 ± 0.06) is statistically different from those of cholesterol-

loaded (0.9 ± 0.03) and unmodified cells (1 ± 0.16), which agrees with experiment 1 results. In addition, cell permeability of cholesterol-depleted cells is significantly lower than that of unmodified and cholesterol-loaded cells.

Experiment 4: There is statistically significant difference in permeability ratio between unmodified (1 ± 0.14 and 1 ± 0.21) and cholesterol-depleted cells (0.43 ± 0.001 and 0.21 ± 0.002) at 0.5 and 1.5 MPa respectively, which agrees with the results from experiment 1 and 3. Same decrease was observed in cell permeability. In addition, at 0.5 and 1.5 MPa no difference in permeability ratio was observed between cholesterol-loaded (1 ± 0.14 and 0.85 ± 0.07 , respectively) and unmodified (1 ± 0.14 and 1 ± 0.21 , respectively) cells in experiment 4, which agrees with the experimental results from experiments 2 and 3 and with cell permeability data. The permeability ratio of cholesterol-loaded cells (1 ± 0.14 and 0.85 ± 0.07 at 0.5 and 1.5 MPa respectively) was significantly higher than that of cholesterol-depleted cells (0.43 ± 0.01 and 0.21 ± 0.02 at 0.5 and 1.5 MPa respectively) in experiment 4, which agrees with the data from experiment 3. Similar statistically significant difference was observed in cell permeability between cholesterol-loaded and cholesterol-depleted cells in experiment 4 (Figure A.4).

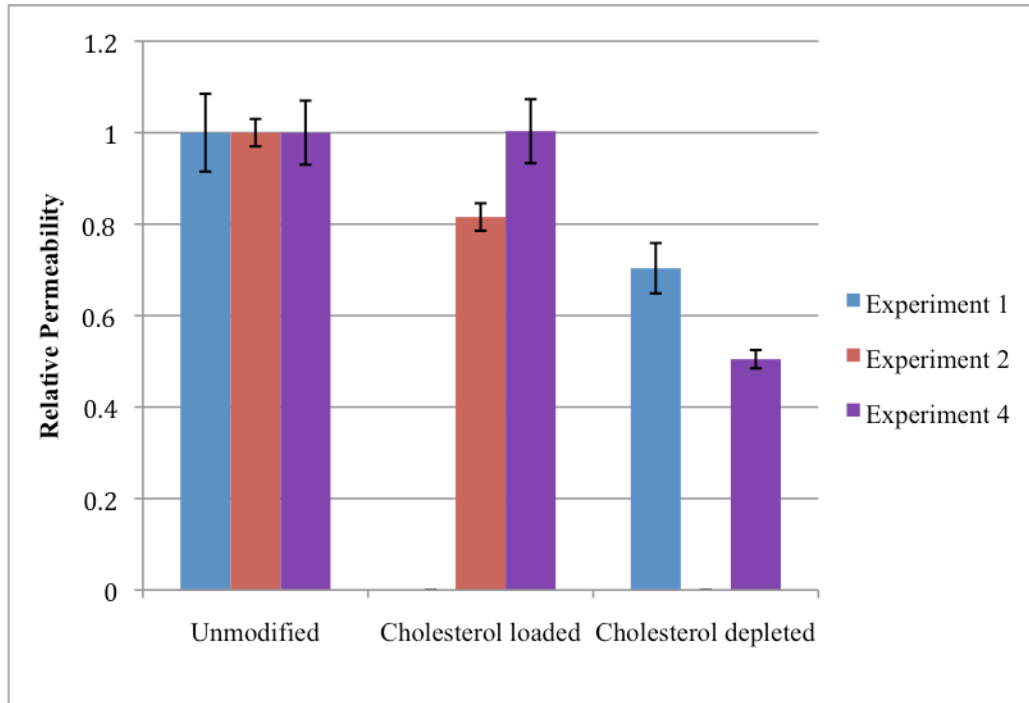


Figure 3.9: The effect of the plasma membrane modification with cholesterol loading and depletion on relative permeability of MDA-MB-231 cells at 0.5 MPa for three independent experiments. Error bars represent standard error of the mean (Experiment 1: $n = 4$, Experiment 2: $n = 8$, Experiment 4: $n = 4$).

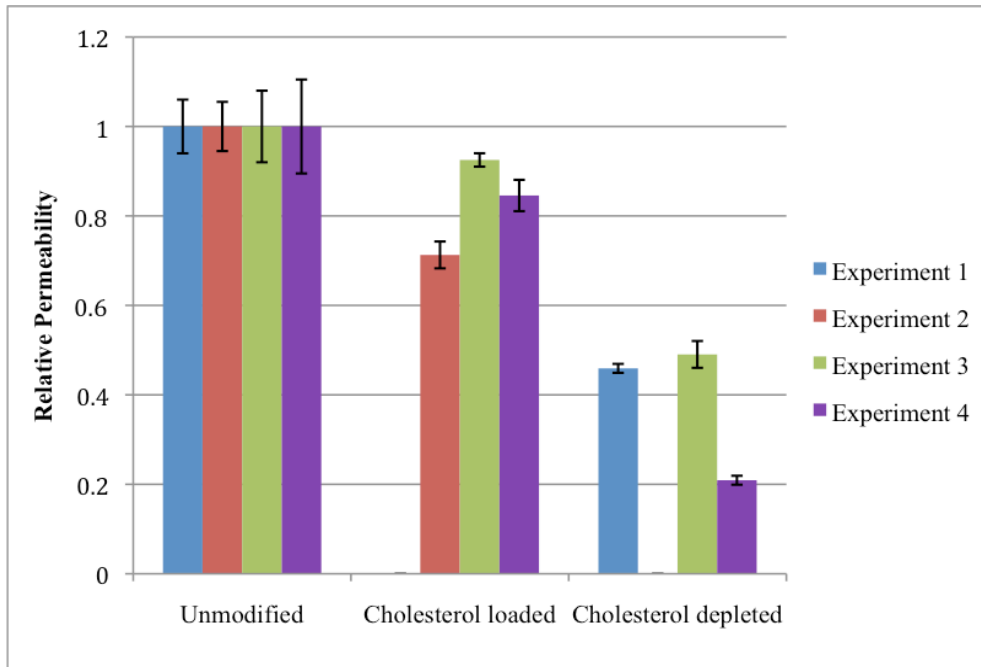


Figure 3.10: The effect of the plasma membrane modification with cholesterol loading and depletion on relative permeability of MDA cells at 1.5 MPa for four independent experiments. Error bars represent standard error of the mean (Experiment 1: $n = 4$, Experiment 2: $n = 8$, Experiment 3: $n = 4$, Experiment 4: $n = 4$).

A.4 Relative Viability of MDA-MB-231 cells

Relative viability for each experiment

Relative viability of unmodified, cholesterol-loaded and cholesterol-depleted MDA-MB-231 cells at 0.5 MPa is plotted for three independent experiments on Figure 3.12 and viability ratio at 1.5 MPa it is plotted for four independent experiments on Figure 3.13.

Experiment 1: In experiment 1 at 0.5 and 1.5 MPa there is no statistically significant difference in viability ratio between unmodified (1 ± 0.04 and 1 ± 0.04 , respectively) and cholesterol-depleted (0.83 ± 0.05 and 1.01 ± 0.06 , respectively) MDA-MB-231 cells on 95 % confidence interval, which agrees with the cell viability results (Figure 3.1).

Experiment 2: In experiment 2 there is statistically significant difference at 0.5 and 1.5 MPa in viability ratio between unmodified (1 ± 0.05 and 1 ± 0.07 , respectively) and cholesterol-loaded (0.83 ± 0.05 and 0.78 ± 0.05 , respectively) MDA-MB-231 cells. Similar decrease was observed in cell viability, however it was not statistically significant (Figure 3.2) at both pressures.

Experiment 3: There is statistically significant difference in viability ratio at 1.5 MPa between unmodified (1 ± 0.04) and cholesterol-loaded (0.84 ± 0.03), unmodified (1 ± 0.04) and cholesterol-depleted (0.56 ± 0.05), as well as between cholesterol-loaded (0.84 ± 0.03) and cholesterol-depleted (0.56 ± 0.05) MDA-MB-231 cells, which agrees with experiment 2 data and disagrees with data from experiment 1. Viability data agrees well with the viability ratio results (Figure 3.3).

Experiment 4: In experiment 4 at 0.5 and 1.5 MPa there is no statistically significant difference in viability ratio between unmodified (1 ± 0.14 , 1 ± 0.22 , respectively) and cholesterol-loaded cells (0.90 ± 0.12 , 0.92 ± 0.05 , respectively), between unmodified (1 ± 0.14 and 1 ± 0.22 , respectively) and cholesterol-depleted (0.96 ± 0.06 and 0.80 ± 0.10 , respectively), and between cholesterol-loaded (0.90 ± 0.12 , 0.92 ± 0.05 , respectively) and cholesterol-depleted (0.96 ± 0.06 and 0.80 ± 0.10 , respectively) MDA-MB-231 cells, which agrees with the cell viability data (Figure 3.4). Similar results were achieved in cell viability ratio in experiment 1. On the contrary, there are statistically significant differences in viability ratio among unmodified and cholesterol-modified MDA-MB-231 cells in experiment 2 and 3.

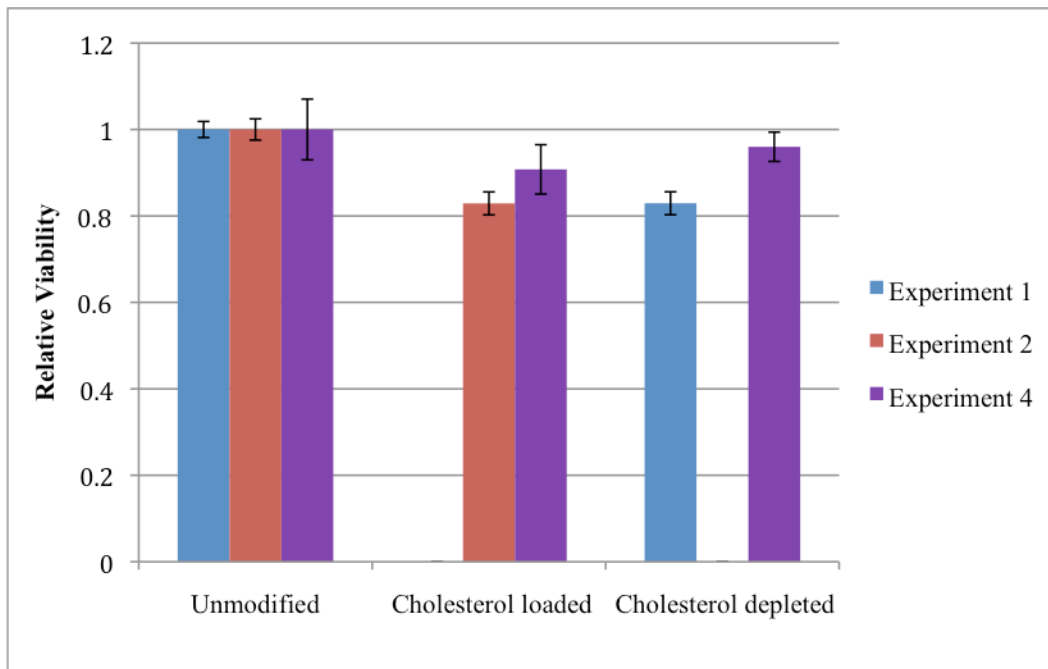


Figure A.11: The effect of the plasma membrane modification with cholesterol loading and depletion on relative viability of MDA-MB-231 cells at 0.5 MPa for three independent experiments. Error bars represent the standard error of the mean (Experiment 1: $n=4$, Experiment 2: $n=8$, Experiment 4: $n=4$).

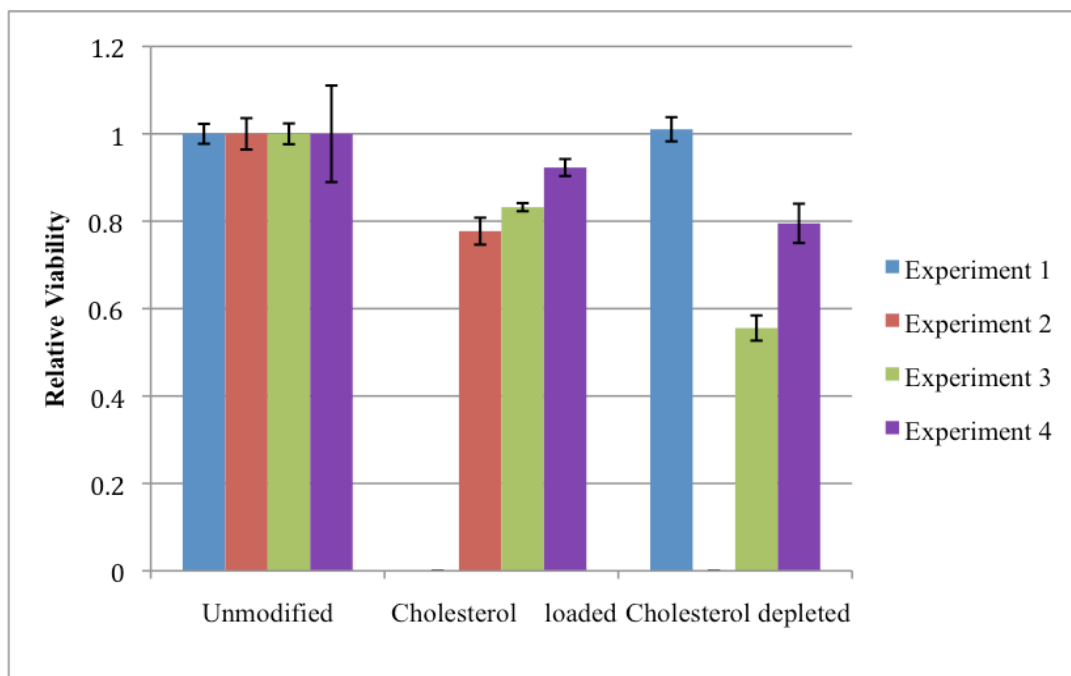


Figure 3.13: The effect of the plasma membrane modification with cholesterol loading and depletion on relative viability of MDA-MB-231 cells at 1.5 MPa for four independent experiments. Error bars represent the standard error of the mean (Experiment 1: $n=4$, Experiment 2: $n=8$, Experiment 3: $n=4$, Experiment 4: $n=4$).

References

Basta, G., Venneri, L., Lazzerini, G., Pasanisi, E., Pianelli, M., Vesentini, N., et al. (2003). In vitro modulation of intracellular oxidative stress of endothelial cells by diagnostic cardiac ultrasound. *Cardiovascular Research*, 58(1), 156-161.

Behnke, O., Tranum-Jensen, J., Van Deurs, B. (1984). Fillipin as a cholesterol probe. Fillipin-cholesterol interaction in red blood cell membranes. *European Journal of Cell Biology*, 35 (2), pp. 200-215.

Bernsdorff, C., Wolf, A., Winter, R., & Gratton, E. (1997). Effect of hydrostatic pressure on water penetration and rotational dynamics in phospholipid-cholesterol bilayers. *Biophysical Journal*, 72(3), 1264-1277.

Bian, A., Gao, Y., Tan, K., Liu, P., Zeng, G., Zhang, X., et al. (2004). Preparation of human hepatocellular carcinoma-targeted liposome microbubbles and their immunological properties. *World Journal of Gastroenterology*, 10(23), 3424-3427.

Blomley, M. (2003). Which US microbubble contrast agent is best for gene therapy? *Radiology*, 229(2), 297-298.

Borden M.A., Kruse D.E., Caskey C.F., Zhao S., Dayton P.A., Ferrara K.W. (2005). Influence of lipid shell physicochemical properties on ultrasound-induced microbubble destruction. *IEEE transactions on ultrasonics, ferroelectrics, and frequency control* 2005, 52, 1992-2002.

Brasitus T.A., Dahiya R., Dudeja P.K. (1988). Bissonnette BM: Cholesterol modulates alkaline phosphatase activity of rat intestinal microvillus membranes. *Journal of Biological Chemistry*, 263, 8592-8597.

Brown MS, Goldstein JL (1986) A receptor-mediated pathway for cholesterol homeostasis. *Science* 232:34-37.

Brujan, E. A. (2004). The role of cavitation microjets in the therapeutic applications of ultrasound. *Ultrasound in Medicine and Biology*, 30(3), 381-387.

Bull, J. L. (2007). The application of microbubbles for targeted drug delivery. *Expert Opinion on Drug Delivery*, 4(5), 475-493.

Cai, X., Xing, X., Cai, J., Chen, Q., Wu, S., & Huang, F. (2010). Connection between biomechanics and cytoskeleton structure of lymphocyte and Jurkat cells: An AFM study. *Micron*, 41(3), 257-262.

Foundations of biomedical ultrasound by Richard S.C. Cobbold. Publisher Oxford; Toronto: Oxford University press, 2007.

Cusack Jr., J. C., & Tanabe, K. K. (2002). Introduction to cancer gene therapy. *Surgical Oncology Clinics of North America*, 11(3), 497-519.

Chapelon JY, Cathigol D, Cain C, Ebbini ES, Kluiwstra JU, Sapozhnikov OA, Fleury G, Berriet R, Chupin L, Guey JL, New piezoelectric transducers for therapeutic ultrasound. *Ultrasound in Medicine and Biology* 2000;26:153-59.

Chapman R. B. & Plesset M. S. (1971). Thermal effects in the free oscillation of gas bubbles. *J Basic Eng Trans ASME*, 93 Ser D(3), 373-376.

Cossec, J., Simon, A., Marquer, C., Moldrich, R. X., Leterrier, C., Rossier, J., et al. (2010). Clathrin-dependent APP endocytosis and A β secretion are highly sensitive to the level of plasma membrane cholesterol. *Biochimica Et Biophysica Acta - Molecular and Cell Biology of Lipids*, 1801(8), 846-852.

Davey, H. M., & Kell, D. B. (1996). Flow cytometry and cell sorting of heterogeneous microbial populations: The importance of single-cell analyses. *Microbiological Reviews*, 60(4), 641-696.

Deng, C. X., Sieling, F., Pan, H., & Cui, J. (2004). Ultrasound-induced cell membrane porosity. *Ultrasound in Medicine and Biology*, 30(4), 519-526.

Dibya, D., Arora, N., & Smith, E. A. (2010). Noninvasive measurements of integrin microclustering under altered membrane cholesterol levels. *Biophysical Journal*, 99(3), 853-861.

Doherty, G. J., & McMahon, H. T. (2009). Mechanisms of endocytosis, *Annual Review in Biochemistry*, 78, 857-902.

Duck A. Francis. Physical properties of tissue

Fahnestock, M., Rimer, V. G., Yamawaki, R. M., Ross, P., & Edmonds, P. D. (1989). Effects of ultrasound exposure in vitro on neuroblastoma cell membranes. *Ultrasound in Medicine and Biology*, 15(2), 133-144.

Fan, X., River, J. N., Muresan, A. S., Popescu, C., Zamora, M., Culp, R. M., et al. (2006). MRI of perfluorocarbon emulsion kinetics in rodent mammary tumours. *Physics in Medicine and Biology*, 51(2), 211-220.

Faria, E. C., Ma, N., Gazi, E., Gardner, P., Brown, M., Clarke, N. W., et al. (2008). Measurement of elastic properties of prostate cancer cells using AFM. *Analyst*, 133(11), 1498-1500.

Ferrara, K., Pollard, R., & Borden, M. (2007). Ultrasound microbubble contrast agents: Fundamentals and application to gene and drug delivery. *Annual Review of Biomedical Engineering*, 9, 415-447.

Frenkel, P. A., Chen, S., Thai, T., Shohet, R. V., & Grayburn, P. A. (2002). DNA-loaded albumin microbubbles enhance ultrasound-mediated transfection in vitro. *Ultrasound in Medicine and Biology*, 28(6), 817-822.

Frenkel, V. (2008). Ultrasound mediated delivery of drugs and genes to solid tumors. *Advanced Drug Delivery Reviews*, 60(10), 1193-1208.

Frenkel, V. (Ed.). (2011). *Therapeutic ultrasound: Mechanisms to applications*. New York: Nova Science Publishers.

Gao, X., Kim, K., & Liu, D. (2007). Nonviral gene delivery: What we know and what is next. *AAPS Journal*, 9(1), art. no. 9.

Gehl, J. (2003). Electroporation: Theory and methods, perspectives for drug delivery, gene therapy and research. *Acta Physiologica Scandinavica*, 177(4), 437-447.

Giacca, M. (2010). *Gene therapy*. Milan: Springer.

Goodwin, J. S., Drake, K. R., Remmert, C. L., & Kenworthy, A. K. (2005). Ras diffusion is sensitive to plasma membrane viscosity. *Biophysical Journal*, 89(2), 1398-1410.

Gleason M.M, Medow M.S., Tulenko T.N. (1991). Excess membrane cholesterol alters calcium movements, cytosolic calcium levels, and membrane fluidity in arterial smooth muscle cells. *Circulation Research* 69(1): 216–227.

Globocan 2008, IARC, 2010. Retrieved from <http://globocan.iarc.fr/factsheets/populations/factsheet.asp?uno=900>.

Ilangumaran, S., & Hoessli, D. C. (1998). Effects of cholesterol depletion by cyclodextrin on the sphingolipid microdomains of the plasma membrane. *Biochemical Journal*, 335(2), 433-440.

Juffermans, L. J. M., van Dijk, A., Jongenelen, C. A. M., Drukarch, B., Reijkerkerk, A., de Vries, H. E., et al. (2009). Ultrasound and microbubble-induced intra- and intercellular bioeffects in primary endothelial cells. *Ultrasound in Medicine and Biology*, 35(11), 1917-1927.

Juffermans, L. J. M., Dijkmans, P. A., Musters, R. J. P., Visser, C. A., & Kamp, O. (2006). Transient permeabilization of cell membranes by ultrasound-exposed microbubbles is related to formation of hydrogen peroxide. *American Journal of Physiology - Heart and Circulatory Physiology*, 291(4), H1595-H1601.

Kaddur, K., Lebegue, L., Tranquart, F., Midoux, P., Pichon, C., & Bouakaz, A. (2010). Transient transmembrane release of green fluorescent proteins with sonoporation. *IEEE Transactions on Ultrasonics, Ferroelectrics, and Frequency Control*, 57(7), 1558-1567.

Kakorin, S., Brinkmann, U., & Neumann, E. (2005). Cholesterol reduces membrane electroporation and electric deformation of small bilayer vesicles. *Biophysical Chemistry*, 117(2), 155-171.

Karshafian, R., Bevan, P. D., Williams, R., Samac, S., & Burns, P. N. (2009). Sonoporation by ultrasound-activated microbubble contrast agents: Effect of acoustic exposure parameters on cell membrane permeability and cell viability. *Ultrasound in Medicine and Biology*, 35(5), 847-860.

Karshafian, R., Samac, S., Bevan, P. D., & Burns, P. N. (2010). Microbubble mediated sonoporation of cells in suspension: Clonogenic viability and influence of molecular size on uptake. *Ultrasonics*, 50(7), 691-697.

Kasza, K. E., Rowat, A. C., Liu, J., Angelini, T. E., Brangwynne, C. P., Koenderink, G. H., et al. (2007). The cell as a material. *Current Opinion in Cell Biology*, 19(1), 101-107.

Kim, J. A., Cho, K., Shin, M. S., Lee, W. G., Jung, N., Chung, C., et al. (2008). A novel electroporation method using a capillary and wire-type electrode. *Biosensors and Bioelectronics*, 23(9), 1353-1360.

Kimmel, E. (2006). Cavitation bioeffects. *Critical Reviews in Biomedical Engineering*, 34(2), 105-16.

- Kinoshita, M., & Hynynen, K. (2005). A novel method for the intracellular delivery of siRNA using microbubble-enhanced focused ultrasound. *Biochemical and Biophysical Research Communications*, 335(2), 393-399.
- Kirk Shung K., Diagnostic ultrasound: imaging and blood flow measurement (2006). Boca Raton, FL: Taylor&Francis.
- Klein, U., Gimpl, G., & Fahrenholz, F. (1995). Alteration of the myometrial plasma membrane cholesterol content with β -cyclodextrin modulates the binding affinity of the oxytocin receptor. *Biochemistry*, 34(42), 13784-13793.
- Kondo, T., Mišík, V., & Riesz, P. (1998). Effect of gas-containing microspheres and echo contrast agents on free radical formation by ultrasound. *Free Radical Biology and Medicine*, 25(4-5), 605-612.
- Koronkiewicz, S., & Kalinowski, S. (2004). Influence of cholesterol on electroporation of bilayer lipid membranes: Chronopotentiometric studies. *Biochimica Et Biophysica Acta - Biomembranes*, 1661(2), 196-203.
- Krasovitski, B., & Kimmel, E. (2001). Gas bubble pulsation in a semiconfined space subjected to ultrasound. *Journal of the Acoustical Society of America*, 109(3), 891-898.
- Kuhry, J., Duportail, G., Bronner, C., & Laustriat, G. (1985). Plasma membrane fluidity measurements on whole living cells by fluorescence anisotropy of trimethylammoniumdiphenylhexatriene. *Biochimica Et Biophysica Acta - Molecular Cell Research*, 845(1), 60-67.
- Kumon, R. E., Aehle, M., Sabens, D., Parikh, P., Kourennyi, D., & Deng, C. X. (2007). Ultrasound-induced calcium oscillations and waves in chinese hamster ovary cells in the presence of microbubbles. *Biophysical Journal*, 93(6), L29-L31.
- Lagerholm, B. C., Weinreb, G. E., Jacobson, K., & Thompson, N. L. (2005). Detecting microdomains in intact cell membranes. *Annual Review of Physical Chemistry*, 56, 309-336
- Larkin, J. O., Casey, G. D., Tangney, M., Cashman, J., Collins, C. G., Soden, D. M., et al. (2008). Effective tumor treatment using optimized ultrasound-mediated delivery of bleomycin. *Ultrasound in Medicine and Biology*, 34(3), 406-413.
- Lars Bastiaanse, E. M., Höld, K. M., & Van Der Laarse, A. (1997). The effect of membrane cholesterol content on ion transport processes in plasma membranes. *Cardiovascular Research*, 33(2), 272-283.

- Lentacker, I., De Smedt, S. C., & Sanders, N. N. (2009). Drug loaded microbubble design for ultrasound triggered delivery. *Soft Matter*, 5(11), 2161-2170.
- Li, T., Tachibana, K., Kuroki, M., & Kuroki, M. (2003). Gene transfer with echo-enhanced contrast agents: Comparison between albumex, optison, and levovist in mice - initial results. *Radiology*, 229(2), 423-428.
- Liang, H., Lu, Q. L., Xue, S., Halliwell, M., Kodama, T., Cosgrove, D. O., et al. (2004). Optimisation of ultrasound-mediated gene transfer (sonoporation) in skeletal muscle cells. *Ultrasound in Medicine and Biology*, 30(11), 1523-1529.
- Liang, H., Tang, J., & Halliwell, M. (2010). Sonoporation, drug delivery, and gene therapy. *Proceedings of the Institution of Mechanical Engineers, Part H: Journal of Engineering in Medicine*, 224(2), 343-361.
- Lim, C. T., Zhou, E. H., & Quek, S. T. (2006). Mechanical models for living cells - A review. *Journal of Biomechanics*, 39(2), 195-216.
- Lindner, J. R. (2004). Microbubbles in medical imaging: Current applications and future directions. *Nature Reviews Drug Discovery*, 3(6), 527-532.
- Liu, D., Ren, T., & Gao, X. (2003). Cationic transfection lipids. *Current Medicinal Chemistry*, 10(14), 1307-1315.
- Madeira, C., Ribeiro, S. C., Pinheiro, I. S. M., Martins, S. A. M., Andrade, P. Z., da Silva, C. L., et al. (2011). Gene delivery to human bone marrow mesenchymal stem cells by microporation. *Journal of Biotechnology*, 151(1), 130-136.
- Marmottant, P., & Hilgenfeldt, S. (2003). Controlled vesicle deformation and lysis by single oscillating bubbles. *Nature*, 423(6936), 153-156.
- Mayer, C. R., & Bekeredjian, R. (2008). Ultrasonic gene and drug delivery to the cardiovascular system. *Advanced Drug Delivery Reviews*, 60(10), 1177-1192.
- Mayer, C. R., Geis, N. A., Katus, H. A., & Bekeredjian, R. (2008). Ultrasound targeted microbubble destruction for drug and gene delivery. *Expert Opinion on Drug Delivery*, 5(10), 1121-1138.
- Meairs, S., & Alonso, A. (2007). Ultrasound, microbubbles and the blood-brain barrier. *Progress in Biophysics and Molecular Biology*, 93(1-3), 354-362.

Mehier-Humbert, S., Bettinger, T., Yan, F., & Guy, R. H. (2005). Plasma membrane poration induced by ultrasound exposure: Implication for drug delivery. *Journal of Controlled Release*, 104(1), 213-222.

Meijering, B. D. M., Henning, R. H., Van Gilst, W. H., Gavrilovic, I., Van Wamel, A., & Deelman, L. E. (2007). Optimization of ultrasound and microbubbles targeted gene delivery to cultured primary endothelial cells. *Journal of Drug Targeting*, 15(10), 664-671.

Meijering, B. D. M., Juffermans, L. J. M., Van Wamel, A., Henning, R. H., Zuhorn, I. S., Emmer, M., et al. (2009). Ultrasound and microbubble-targeted delivery of macromolecules is regulated by induction of endocytosis and pore formation. *Circulation Research*, 104(5), 679-687.

Meunier, J. M., Holland, C. K., Lindsell, C. J., & Shaw, G. J. (2007). Duty cycle dependence of ultrasound enhanced thrombolysis in a human clot model. *Ultrasound in Medicine and Biology*, 33(4), 576-583.

Miller, M. W., Everbach, E. C., Miller, W. M., & Battaglia, L. F. (2003). Biological and environmental factors affecting ultrasound-induced hemolysis in vitro: 2. medium dissolved gas (pO₂) content. *Ultrasound in Medicine and Biology*, 29(1), 93-102.

Miller, D. L., Pislaru, S. V., & Greenleaf, J. F. (2002). Sonoporation: Mechanical DNA delivery by ultrasonic cavitation. *Somatic Cell and Molecular Genetics*, 27(1-6), 115-134.

Mizutani, Y., Tsuchiya, M., Hiratsuka, S., Kawahara, K., Tokumoto, H., & Okajima, T. (2008). Elasticity of living cells on a microarray during the early stages of adhesion measured by atomic force microscopy. *Japanese Journal of Applied Physics*, 47(7 PART 3), 6177-6180.

Mukherjee, D., Wong, J., Griffin, B., Ellis, S. G., Porter, T., Sen, S., et al. (2000). Ten-fold augmentation of endothelial uptake of vascular endothelial growth factor with ultrasound after systemic administration. *Journal of the American College of Cardiology*, 35(6), 1678-1686.

Needham, D., McIntosh, T. J., & Evans, E. (1988). Thermomechanical and transition properties of dimyristoylphosphatidylcholine/cholesterol bilayers. *Biochemistry*, 27(13), 4668-4673.

Nelson David L., & Cox Michael M. (Eds.). (2008). *Principles of biochemistry* (5th ed.). New York: W.H.Freeman and company.

Nomikou, N., & McHale, A. P. (2010). Exploiting ultrasound-mediated effects in delivering targeted, site-specific cancer therapy. *Cancer Letters*, 296(2), 133-143.

Nozaki, T., Ogawa, R., Feril Jr., L. B., Kagiya, G., Fuse, H., & Kondo, T. (2003). Enhancement of ultrasound-mediated gene transfection by membrane modification. *Journal of Gene Medicine*, 5(12), 1046-1055.

Ohl, C., Arora, M., Ikink, R., De Jong, N., Versluis, M., Delius, M., et al. (2006). Sonoporation from jetting cavitation bubbles. *Biophysical Journal*, 91(11), 4285-4295.

Pan, H., Zhou, Y., Izadnegahdar, O., Cui, J., & Deng, C. X. (2005). Study of sonoporation dynamics affected by ultrasound duty cycle. *Ultrasound in Medicine and Biology*, 31(6), 849-856.

Pitha, J., Irie, T., Sklar, P. B., & Nye, J. S. (1988). Drug solubilizers to aid pharmacologists: Amorphous cyclodextrin derivatives. *Life Sciences*, 43(6), 493-502.

Qin, S., Caskey, C. F., & Ferrara, K. W. (2009). Ultrasound contrast microbubbles in imaging and therapy: Physical principles and engineering. *Physics in Medicine and Biology*, 54(6), R27-R57.

Rapoport, N. Y., Kennedy, A. M., Shea, J. E., Scaife, C. L., & Nam, K. -. (2009). Controlled and targeted tumor chemotherapy by ultrasound-activated nanoemulsions/microbubbles. *Journal of Controlled Release*, 138(3), 268-276.

Rodal, S. K., Skretting, G., Garred, Ø., Vilhardt, F., Van Deurs, B., & Sandvig, K. (1999). Extraction of cholesterol with methyl- β -cyclodextrin perturbs formation of clathrin-coated endocytic vesicles. *Molecular Biology of the Cell*, 10(4), 961-974.

Rols, M. P., Dahhou, F., Mishra, K. P., & Teissié, J. (1990). Control of electric field induced cell membrane permeabilization by membrane order. *Biochemistry*, 29(12), 2960-2966.

Ross, J. P., Cai, X., Chiu, J., Yang, J., & Wu, J. (2002). Optical and atomic force microscopic studies on sonoporation. *Journal of the Acoustical Society of America*, 111(3), 1161- 1164.

Schlicher, R. K., Hutcheson, J. D., Radhakrishna, H., Apkarian, R. P., & Prausnitz, M. R. (2010). Changes in cell morphology due to plasma membrane wounding by acoustic cavitation. *Ultrasound in Medicine and Biology*, 36(4), 677-692.

- Schlicher, R. K., Radhakrishna, H., Tolentino, T. P., Apkarian, R. P., Zarnitsyn, V., & Prausnitz, M. R. (2006). Mechanism of intracellular delivery by acoustic cavitation. *Ultrasound in Medicine and Biology*, 32(6), 915-924.
- Sheguang Zhang, Duncan, J. H., & Chahine, G. L. (1993). The final stage of the collapse of a cavitation bubble near a rigid wall. *Journal of Fluid Mechanics*, 257, 147-181.
- Schwarz S.M., Bostwick H.E., Medow M.M. (1988). Estrogenmodulates ileal basolateral membrane lipid dynamics and Na⁺/K⁺-ATPase activity. *American Journal of Physiology*, 254, G687-G694.
- Simberg, D., & Mattrey, R. (2009). Targeting of perfluorocarbon microbubbles to selective populations of circulating blood cells. *Journal of Drug Targeting*, 17(5), 392-398.
- Singer, S. J., & Nicolson, G. L. (1972). The fluid mosaic model of the structure of cell membranes. *Science*, 175(4023), 720-731.
- Szabo Thomas L. Diagnostic ultrasound imaging: inside out (2004). Boston: Elsevier/Academic Press.
- Tallima, H., El Ridi, R. (2005). Methyl- β -cyclodextrin treatment and filipin staining reveal the role of cholesterol in surface membrane antigen sequestration of *Shistosoma mansoni* and *S. haematobium* lung-stage larvae. *Journal of Parasitology*, 91 (3), pp. 720-725.
- Taniyama, Y., Tachibana, K., Hiraoka, K., Namba, T., Yamasaki, K., Hashiya, N., et al. (2002). Local delivery of plasmid DNA into rat carotid artery using ultrasound. *Circulation*, 105(10), 1233-1239.
- Torchilin, V. P. (2006). Recent approaches to intracellular delivery of drugs and DNA and organelle targeting. *Annual Review of Biomedical Engineering*, 8, 343-375.
- Ueda, I., Chiou, J., Krishna, P. R., & Kamaya, H. (1994). Local anesthetics destabilize lipid membranes by breaking hydration shell: Infrared and calorimetry studies. *Biochimica Et Biophysica Acta - Biomembranes*, 1190(2), 421-429.
- Upham, B. L., & Trosko, J. E. (2009). Oxidative-dependent integration of signal transduction with intercellular gap junctional communication in the control of gene expression. *Antioxidants and Redox Signaling*, 11(2), 297-307.

Wang Binghe, Siahaan Teruna, & Soltero Richard A. (Eds.). (2005). *Drug delivery principles and applications* (New Jersey ed.) John Willey & Sons, Inc.

Wang, X., Liang, H., Dong, B., Lu, Q., & Blomley, M. J. K. (2005). Gene transfer with microbubble ultrasound and plasmid DNA into skeletal muscle of mice: Comparison between commercially available microbubble contrast agents. *Radiology*, 237(1), 224-229.

Ward, K. A., Li, W., Zimmer, S., & Davis, T. (1991). Viscoelastic properties of transformed cells: Role in tumor cell progression and metastasis formation. *Biorheology*, 28(3-4), 301-313.

Ward, M., Wu, J., & Chiu, J. (1999). Ultrasound-induced cell lysis and sonoporation enhanced by contrast agents. *Journal of the Acoustical Society of America*, 105(5), 2951-2957.

Ward, M., Wu, J., & Chiu, J.(2000). Experimental study of the effects of optison® concentration on sonoporation in vitro. *Ultrasound in Medicine and Biology*, 26(7), 1169-1175.

Warrington Jr., K. H., & Herzog, R. W. (2006). Treatment of human disease by adeno-associated viral gene transfer. *Human Genetics*, 119(6), 571-603.

Whetton A.D., Gordon L.M., Housley M.D. (1983). Elevated membrane cholesterol concentrations inhibit glucagon-stimulated adenylate cyclase. *Biochemistry Journal* 210, 437-449.

Yang, N., Burkholder, J., Roberts, B., Martinell, B., & McCabe, D. (1990). In vivo and in vitro gene transfer to mammalian somatic cells by particle bombardment. *Proceedings of the National Academy of Sciences of the United States of America*, 87(24), 9568-9572.

Yu T, Wang Z, Mason T, A review of research into the uses of low level ultrasound in cancer therapy. *Ultrasonics sonochemistry* 2004;11:95-103.

Zhang, G., Gao, X., Song, Y. K., Vollmer, R., Stolz, D. B., Gasiorowski, J. Z., et al. (2004). Hydroporation as the mechanism of hydrodynamic delivery. *Gene Therapy*, 11(8), 675-682.

Zhang, Z., Xia, C., Xue, Y., & Liu, Y. (2009). Synergistic effect of low-frequency ultrasound and low-dose bradykinin on increasing permeability of the blood-tumor barrier by opening tight junction. *Journal of Neuroscience Research*, 87(10), 2282-2289.

Zhao, Y., Luo, Y., Lu, C., Xu, J., Tang, J., Zhang, M., et al. (2008). Phospholipids-based microbubbles sonoporation pore size and reseal of cell membrane cultured in vitro. *Journal of Drug Targeting*, 16(1), 18-25.